STATISTICAL ANALYSIS OF COGNITIVE SIGNALS MEASURED BY fNIRS

by

Rifat Koray Çiftçi

BS, in Electrical and Electronic Engineering, Boğaziçi University, 1996

MS, in Biomedical Engineering, Boğaziçi University, 2001

Submitted to the Institute of Biomedical Engineering

in partial fulfillment of the requirements

for the degree of

Doctor

of

Philosophy

Boğaziçi University

June 2008

ACKNOWLEDGMENTS

I would like to express my deep gratitudes to my thesis supervisor Prof. Yasemin P. Kahya for her everlasting support and understanding. Her generous reliance on me always gave the motivation and energy that I needed in hard times. I will keep the things that I learned from her throughout the rest of my life.

I would like to thank my thesis cosupervisor Prof. Ata Akın for persuading me to take part in this exciting research area. He guided me not to be drown in numbers and symbols and not to lose connection with practice. His door was always open when I had some questions to ask.

Throughout this thesis study, the enthusiasm of one person was perhaps higher than me: Prof. Bülent Sankur always challenged me to go to the utmost point. To be a witness of his scientific methodology and scientific interest were definitely two of the most important benefits of this thesis study for me.

I was lucky to share the same laboratory with Mete Yeğiner and İpek Şen. I owe much to the harmonious group that we formed and the happy atmosphere in the laboratory that people always admire. I would like to thank to my dear colleagues for their contributions in the completion of this dissertation.

My eternal friend Helin Dutağacı provided me with some fresh air when I needed in this small "village." I would like to thank her for everything we shared during these long years of research.

Prof. Kubilay Aydın is an important figure in my scientific research record. I saw my name in a journal paper as an author for the first time with the studies that we have done together. The experience that I have gained from those studies helped me a lot during my doctoral research.

I am indebted to all of the members of the Institute of Biomedical Engineering. It was a priviledge for me to be a member of BME. I, particularly, want to thank Burteçin, Uzay and Ömer for the discussions that we have made on "photons, hemoglobins and so on."

My mother, father and sister... I don't want to miss this chance to say a big "thank you" to them. This dissertation is one of the biggest things I managed to do in my life and I want to think of it as a present to them for all the things that they have done for me.

The last two years of my life were extraordinary in many ways. soL, alone, was enough to turn my life into an irrational character. Perhaps, ironically, this "irrationality" make it easier for me to finish this dissertation. I would like to thank all of the soL workers for their invaluable contributions in enriching my life. The other "irrational" ingredient of my life in these two years was marriage. Zeynep, I still don't know how, managed to manufacture a new version of me that has definitely less bugs. Then, everything was so easy... Thank you.

ABSTRACT

STATISTICAL ANALYSIS OF COGNITIVE SIGNALS MEASURED BY fNIRS

Further standardization in signal processing tools is needed in the area of functional near infrared spectroscopy (fNIRS) before it is recognized as a reliable neuroimaging modality. This thesis study attempts to present a comprehensive analysis of the feasibility of applying statistical inference methods to fNIRS signals. Using hierarchical linear models, both classical and Bayesian techniques are pursued and performances of different methods are presented on a comparative basis. The results obtained from a set of cognitive signals show that fNIRS can identify cognitive activity both at the subject and group levels. The analysis suggests that mixed or Bayesian hierarchical models are especially convenient for fNIRS signals. A related problem that is discussed in this thesis study is to relate the outcome of the statistical analysis with the underlying physiology. This problem is studied by putting constraints over the parameters to be estimated. Carrying the problem to a Bayesian framework, the constraints were turned into prior distributions and Gibbs sampling was used to infer from the posterior distributions. The results exhibit that in addition to preventing unlikely results to appear at the end of the analysis, using parameter constraints is also more efficient in revealing activations which are obscured by heavy noise. The last part of this thesis study departs from hypothesis-based statistical inference techniques and introduces the use of information-theoretic measures for fNIRS by particularly concentrating on neural complexity and functional clustering. It is demonstrated that this type of measures may capture organizational aspects of the brain which are hard to reveal with classical statistical inference techniques.

Keywords: Functional near infrared spectroscopy, Statistical inference, Bayesian statistics, General linear model, Constrained estimation, Complexity.

ÖZET

iYKAS İLE ÖLÇÜLMÜŞ BİLİŞSEL SİNYALLERİN İSTATİSTİKSEL ANALİZİ

İşlevsel yakın kırmızıaltı spektroskopi'nin (iYKAS) güvenilir bir nörogörüntüleme yöntemi olarak kabul edilebilmesi için sinyal işleme teknikleri açısından bir standartlaştırmaya ihtiyaç vardır. Bu tez çalışması istatistiksel çıkarsama yöntemlerinin iYKAS sinyallerine uygulanmasının kapsamlı bir olurluk incelemesini yapmayı amaçlamıştır. Sıradüzensel doğrusal modeller kullanılarak, hem klasik hem de Bayesçi çerçevede değişik yöntemlerin başarımı karşılaştırmalı olarak sunulmuştur. Bilişsel bir deney sırasında ölçülen sinyallerden elde edilen sonuçlar iYKAS'ın hem denek hem de grup seviyesinde bilişsel aktiviteyi belirleyebildiğini göstermiştir. Yapılan analizler karışık ya da Bayesçi sıradüzensel modellerin iYKAS sinyalleri için daha uygun olduğunu ortaya koymuştur. Bununla ilintili olarak bu tez çalışmasında tartışılan diğer bir problem istatistiksel analizin sonuçlarının altta yatan fizyolojiyle uyumunun garanti edilmesidir. Bu problem kestirilecek parametreler üzerinde kısıtlar koyulmasıyla ele alınmıştır. Ardından problemi Bayesçi bir çerçeveye taşıyarak kısıtlar önsel dağılımlara dönüştürülmüş ve Gibbs örneklemesi kullanılarak sonsal dağılımlar üzerinden çıkarsama yapılmıştır. Sonuçlar, parametre kısıtları koymanın, analizin sonucunda olası olmayan sonuçlar çıkmasını engellemenin yanı sıra ağır gürültüyle örtülmüş aktivitelerin de ortaya çıkarılması için daha etkin olduğunu ortaya koymuştur. Tezin son bölümü hipotez temelli istatistiksel çıkarsama tekniklerinden uzaklaşmakta ve bilgi-kuramsal ölçütlerin iYKAS için kullanımına giriş yapmaktadır. Bunu yaparken özellikle nöral karmaşıklık ve işlevsel topaklandırma üzerinde yoğunlaşılmış ve bu tip ölçütlerin beynin örgütleşimine ilişkin klasik istatistiksel çıkarsama yöntemleriyle fark edilmesi güç yönleri yakalayabildiği gösterilmiştir.

Anahtar Sözcükler: Yakın kırmızıaltı spektroskopi, İstatistiksel çıkarsama, Bayesçi istatistik, Sıradüzensel doğrusal model, Kısıtlı kestirim, Karmaşıklık.

TABLE OF CONTENTS

LIST OF FIGURES

LIST OF SYMBOLS

A	Extinction of light
b_g	Group parameter vector
b_k^c	Concatenated parameter vector
b	Vector of parameters of interest
$\mathcal{B}$	Differential pathlength factor
B_g	Multivariate group parameter vector
C_g	Group level error covariance matrix
e	Error vector
$\mathcal{G}$	Scattering term
h	Vector of parameters for nuisance effects
I_o	Incident light
I_L	Transmitted light
X_g	Group-level design matrix
X_g^m	Multivariate group-level design matrix
X_k^c	Concetanated design matrix
X	Design matrix
Y	fNIRS data vector
Z	Matrix modeling the nuisance effects
ϵ	Extinction coefficient
Φ	Between-subjects covariance matrix
σ^2	Noise variance
Σ	Within-subject covariance matrix
Θ	A multielement neural system
Θ_j^k	j^{th} subset of Θ with k elements

LIST OF ABBREVIATIONS

ACC	Anterior cingulate cortex
BCI	Brain computer interface
BOLD	Blood oxygenation level dependent
BPE	Bayesian posterior estimation
cHRF	Canonical hemodynamic response function
CBF	Cerebral blood flow
CBV	Cerebral blood volume
CI	Cluster index
Deoxy-Hb	Deoxygenated hemoglobin
DPF	Differential pathlength factor
DD	Dispersion derivative
EEG	Electroencephalography
FFX	Fixed effects
fMRI	Functional magnetic resonance imaging
fNIRS	Functional near infrared spectroscopy
GLM	General linear model
H	Entropy
HR	Heart rate
HRF	Hemodynamic response function
I	Integration
ICM	Iterated conditional modes
LED	Light emitting diode
MEG	Magnetoencephalography
MA	Mental arithmetic
MFX	Mixed effects
MI	Mutual information
NHSTP	Null hypothesis significance test procedure
NIRS	Near infrared spectroscopy

C_N	Neural complexity
OLS	Ordinary least squares
Oxy-Hb	Oxygenated hemoglobin
PSA	Parametric statistical analysis
ΨFX	Pseudomixed effects
RFX	Random effects
RT	Reaction time
TD	Temporal derivative

1. INTRODUCTION

Near infrared spectroscopy (NIRS) opened up a new path in the quest for understanding the functioning of the brain. After its introduction as a tool for measuring average tissue oxygen saturation and total hemoglobin concentration [1], increasing number of researchers have started using NIRS for observing cognitive activity. Bearing the name functional near infrared spectroscopy (fNIRS), the method was used for studying the basic functions of the prefrontal cortex [2, 3, 4, 5], motor cortex [6, 7, 8, 9] and visual cortex [10, 11, 12, 13]. Besides these studies on healthy subjects, fNIRS has been employed for exploring neural underpinnings of psychiatric disorders [14, 15, 16, 17]. fNIRS was even used for studying cognitive mechanisms involved in emotion processing [18, 19, 20]. With the growing interest in building brain-computer interfaces (BCI) in the recent years, the feasibility of employing fNIRS in this area has also been put under investigation [21, 22, 23, 24].

The drive of the researchers towards using fNIRS in these broad areas of research was mainly motivated by several potential advantages of fNIRS over other neuroimaging modalities. fNIRS shares much in common with the blood oxygenation level dependent (BOLD) signal of functional magnetic resonance imaging (fMRI) and measures the concentration changes of oxygenated and deoxygenated hemoglobin (oxy-Hb and deoxy-Hb) resulting from the hemodynamic response. Moreover, both fNIRS and fMRI are indirect measures of brain activity. Besides these similarities, fNIRS offers the researchers the possibility of making measurements in various clinical and natural environments. Unlike fMRI, which necessitates bulky and heavy equipments which limit the movements of the subjects, fNIRS devices are relatively user-friendly and portable. This aspect is especially important in the ability to observe cognitive activities with minimum disturbance to the subject. It is even possible to build wireless fNIRS devices [25, 26]. The advantages of fNIRS may further be extended to the absence of radiation, the low cost of the procedure and the ability to measure both oxy-Hb and deoxy-Hb simultaneously. However, as with the rest of the modalities, fNIRS also comes with its

inherent limitations. The major drawbacks of fNIRS may be listed as its low spatial resolution ($1cm^2$), shallow depth of penetration and consequently inevitable uncertainty about the probed region.

The increasing use of fNIRS as a neuroimaging modality brings with itself the need for reliable and efficient procedures to analyze and interpret the observed data. Although there are efforts in this line, [27], there is yet no standard method to process fNIRS data. The goal of this thesis study may be stated in broadest terms as making a contribution to the efforts for building a framework for analyzing fNIRS data.

Neuroimaging generally works with statistical models which make explicit assumptions about data. As long as these assumptions hold, statistics is an effective way to separate the noise from the signal. On the other hand, limitations of statistical analysis should also be noted [28]. This thesis is devoted to the investigation of the feasibility of applying statistical models to fNIRS signals. Main body of the thesis is related with one of the most common types of statistical models, that is general linear model (GLM). Due to its simple and valid assumptions, GLM is the most preferred method for making statistical inference from fMRI data [29]. In addition to its computational simplicity, GLM also lends itself easily to hierarchical structures which may be employed for making group level inferences. Consequently, one of the main goals of this thesis is to employ hierarchical GLMs for making subject and group level inferences from fNIRS data.

Classical inference from neuroimaging data proceeds with null hypothesis significance test procedure (NHSTP). The researcher is not allowed to ask questions directly regarding the probability distribution of the variable of interest. Rather, the null hypothesis is tested and the decision whether to reject it or not is given based on the significance. Bayesian methodology, on the other hand, provides the researchers with necessary tools for exploring the posterior probability distributions of the variables. In this thesis, classical and Bayesian methods for analyzing GLM are investigated in a comparative basis.

Although the general emphasis of this thesis is on model-based analysis, the separation of signal from noise problem is also discussed within an information-theoretic framework. For this purpose, complexity measures are applied with the assumption that cognitive activity causes a change in the interaction type among the brain regions. Conjecturing that this change manifests itself in terms of a change in "complexity", a number of approaches are discussed and evaluated for fNIRS modality. The main difference of these methods from the aforementioned GLM based techniques is that there is no a priori temporal or spatial model. Hence, a wide variety of "structures" can be revealed using complexity measures. However, the cost is that the strict control over the physiological plausibility is lost.

The plausibility of the analysis is generally an overlooked necessity in neuroimaging. With the increasing elasticity of the models, there appears to be a risk of arriving at results which are not physiologically probable. This study approaches the aforementioned problem for GLM-based analysis and proposes a simple way for making statistical inference under parameter contraints which guarantees the plausibility of the estimates.

In summary, this thesis study aims at making three concrete contributions: i) In depth analysis of multilevel statistical inference techniques for fNIRS, ii) A method for making GLM analysis under parameter constraints, iii) Application of information-theoretic measures to fNIRS. These three contributions will be explained in three separate chapters which are preceded with a background information on near infrared spectroscopy and followed by general conclusions and perspectives for future research.

2. NEAR INFRARED SPECTROSCOPY

Photons travelling through a tissue undergo mainly two types of interactions with the tissue: Absorption and scattering. Both of these events cause attenuation in the energy of the light passing through the tissue and this attenuation forms the basis for optical apparatus used for probing the tissue. Imaging devices use sender-receiver pairs for sending the light at some point and receiving it at some other point after it is transmitted or reflected through the tissue. The concentration of a light absorbing molecule in tissues may be determined by the Beer-Lambert Law:

$$A = \epsilon.c.d \tag{2.1}$$

where $A = log(I_o/I_L)$ is the extinction of light which is proportional to the incident (I_o) versus measured light (I_L), ϵ is the extinction coefficient, c is the substance concentration, and d is the distance from source to detector. Beer-Lambert Law assumes infinitesimal substance concentrations and therefore negligible light scattering. However, in real cases, substance concentrations are higher and Eq. 2.1 should be modified to take into account extra loss of light and longer pathlength of the photons due to scattering. Therefore, in the modified Beer-Lambert Law [30], a multiplicative term $(\mathcal{B})$ and an additive term $(\mathcal{G})$ which account for longer pathlength and loss of light, respectively, are added:

$$A = \epsilon.c.d.\mathcal{B} + \mathcal{G} \tag{2.2}$$

Generally the concern is the difference between the two situations and assuming constant light scattering, $\mathcal{G}$ term cancels due to subtraction:

$$\Delta A = \epsilon.\Delta c.d.\mathcal{B} \tag{2.3}$$

If the pathlength factor, $\mathcal{B}$, is known then it is possible to calculate absolute concentrations. The ignorance about the pathlength and the actual path of the pho-

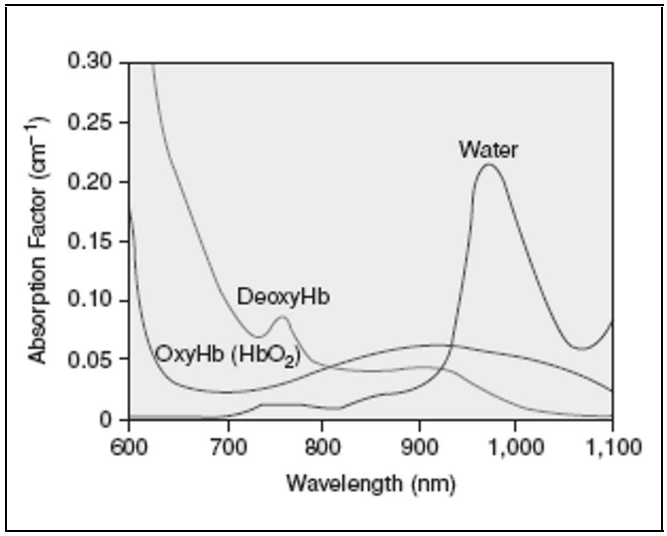

Figure 2.1 Absorption characteristics of oxy-Hb, deoxy-Hb and water [26].

tons are the major drawbacks of the optical imaging. There are different methods for determining the pathlength: One is to measure the time of flight of a very short (in the order of pico seconds) light pulse traveling through the tissues [31]. Another approach is to measure the phase shift of a light source which is intensity-modulated at a certain frequecy [32]. If it is not possible to determine the pathlength then the measurements obtained by optical imaging are relative. There are studies which experimentally determine optical pathlengths for different subject groups, [32], and these values are widely used by the researchers.

Biological tissues are relatively transparent to light in the near infrared range between 700 and 1000 nm, largely because water which is the greatest component in the tissues, relatively absorbs little at these wavelengths (see Figure 2.1). NIRS uses light sources with wavelengths in the near infrared region to observe concentration changes of oxy-Hb and deoxy-Hb within the probed tissues. In addition to changes at the intracellular level, which are hard to observe with NIRS, local brain activity causes an increase in cerebral blood volume (CBV) and cerebral blood flow (CBF). At the capillary level CBF increase is accomplished by higher blood per capillary which is associated with higher blood velocity. During this process, termed as neurovascular coupling [33], the increase in CBF and oxygen delivery exceeds the local consumption of oxygen and cerebral blood oxygenation rises in the activation area. Because oxy-Hb

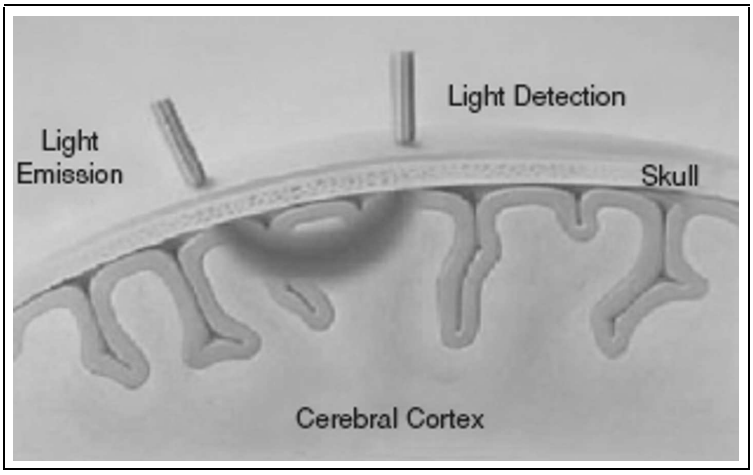

Figure 2.2 Banana-shaped photon path [26].

and deoxy-Hb have characteristic optical properties, it is possible to measure their concentration changes during neurovascular coupling using modified Beer-Lambert Law.

fNIRS devices introduce photons to the scalp through light emitting diodes or lasers. Since large amount of the photons follow a banana shaped path, it is possible to detect them as they leave the head by photodetectors, as illustrated in Figure 2.2. It may be noticed that photons spend a considerable amount of time in non-cerebral tissues, such as skin, skull and cerebrospinal fluid. Consequently, the total absorption measured by a photodetector has significant contributions from these tissues. For continuous-wave systems which does not have a depth-resolution ability, wavelengths of the device and experimental paradigms should be selected and designed so as to minimize this non-cerebral contribution.

A continuous-wave fNIRS device (NIROXCOPE 301) built in Biophotonics Laboratory of Boğaziçi University [34, 35, 36] was used in this study. The device is capable of transmitting near-infrared light at two wavelengths (730 nm and 850 nm). Calculation of concentration changes of oxy-Hb and deoxy-Hb in blood is based on modified Beer-Lambert Law which is summarized by Eq. 2.2 and Eq. 2.3. Employing four light emitting diodes (LEDs) and 10 detectors, the device can sample 16 different volumes in the brain simultaneously (see Figure 2.3 for the details of the probe).

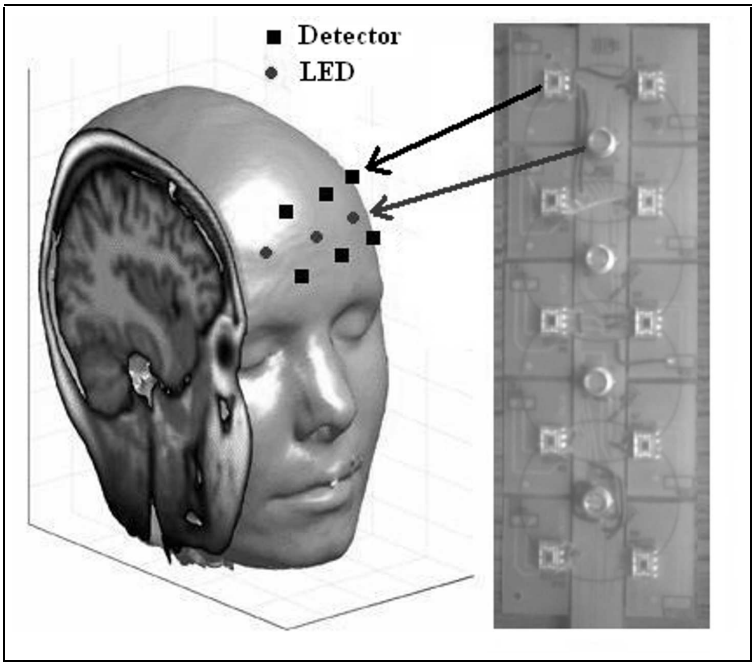

Figure 2.3 NIROXCOPE 301 probe (on the right) is attached to the forehead. Source-detector geometry ensures probing of un-overlapped 16 volumes when the light sources are time multiplexed. (Head image was obtained from MATLAB Central File Exchange).

The rectangular probe geometry was chosen for obtaining non-overlapping areas. Source-to-detector distances was specified as 2.5 cm, since this amount of separation has been shown to reliably probe the cortical activity [37, 38, 39, 40]. LEDs and detectors were placed in a flexible printed circuit board that was specially designed to fit the curvature of the forehead. Sampling frequency of the device was 1.4 Hz.

3. MULTILEVEL STATISTICAL INFERENCE FROM fNIRS SIGNALS

Parametric statistical analysis (PSA) of neuroimaging data tries to answer the question of whether the measured data significantly carry components representative of cognitive activity or not. In the hypothesis-based approach, this investigation begins with tailoring the components that will be searched for. In fMRI and fNIRS this component is hemodynamic response function (HRF). Based on the past research and experimental studies, an HRF model is used to generate hypothetical cognitive components. Then the task is to test if this hypothetical component is captured by the real data. Statistics enters into play at this point. Beginning with some statistical assumptions about data and noise, PSA produces estimates and their associated probabilities for the parameters which are to be inferred on.

Neuroimaging typically works with groups of subjects. The goal may be to reveal the average activity of these subjects or to find the activity differences between two groups of subjects. Consequently, the hypothesis should be answered at the highest level of the hierarchy. This highest level often represents the effect analysis over some or all of several measurements, detectors, sessions and subjects in a population. GLM has been the most commonly used tool to make inferences from fMRI data [29]. GLM may also be extended to a hierarchical mode to arrive at multilevel statistical inferences [41, 42]. In recent years, hierarchical GLM has arisen as an effective tool for proceeding from the data at the subject level to higher levels.

Apart from a few inherent differences between them, both fMRI and fNIRS aim to detect and localize brain hemodynamic activity based upon neurovascular coupling model. Thus, it would be logical to extend the GLM methodology to fNIRS signals. This was first attempted using a visual stimulus and the conclusion was that the GLM type of analysis was feasible especially for deoxy-Hb [27]. In another study, it was shown that model-based analysis with GLM is capable of detecting event-related human brain

activity recorded with fNIRS in the occipital cortex [43]. A *shift method* has also been proposed to recover small signals within the GLM framework, by exploiting the higher temporal resolution of fNIRS with respect to fMRI [44]. In summary, these studies provided us with promising but not conclusive results.

3.1 Statistical Analysis of the Hierarchical GLM

In this thesis study, the multilevel statistical inference problem for fNIRS signals has also been addressed using a hierarchical GLM to link the measurement space to the upper-level parameters. The expositions presented in this chapter are based on [45]. A comparative approach was adopted and three classical methods of multilevel inference, namely, fixed effects (FFX), random effects (RFX), mixed effects (MFX) analyses, and two Bayesian inference methods were implemented simultaneously. One of the Bayesian methods also goes by the name of pseudo-mixed effects (ΨFX) [46], since it employs the basic GLM at the subject level and uses the Bayesian methodology to merge the subject parameters at the group level. The second method, denoted as Bayesian posterior estimation (BPE), is a fully Bayesian one.

3.1.1 Classical Inference

Classical analysis of multilevel functional neuroimaging data generally proceeds in a bottom-up fashion. Once the statistics that summarize the data at one level are calculated, they are carried to the upper level. The main difference among the three classical statistical inference techniques of FFX, RFX and MFX lies in the determination of the variance estimates [47, 48]. Details of the classical inference is given in Appendix A. Briefly, FFX and RFX ignore the between-subject and within-subject variances, respectively. Note that, since it ignores the between-subject variance, the inference of FFX is limited to the particular set of subjects. After calculating the subject parameter and variance estimates using GLM specifically designed for each subject, FFX takes the average variance estimate as the group variance. On the other

hand, RFX calculates the group variance over the estimated parameters of the subjects. MFX tries to integrate both within and between-subject variances by carrying the subject variance estimates to the group level.

In this study, MFX was carried on as described in [47] and implemented in [49]. FFX, RFX and MFX are all summary statistical approaches, that is, beginning from the bottom level, each level is analyzed separately and only the parameters of interest are carried to the upper level. The main benefit of working with a summary statistics approach is its computational ease, which becomes very important for high dimensional data like fMRI.

The statistics proposed by [46], called pseudo-mixed effects (ΨFX), is a mixture of classical and Bayesian procedures. The parameter and variance estimates are calculated at the subject level using the GLM. Then to arrive at the group decision, the posterior distribution of one subject is taken as the prior distribution of another subject. The end result is an average of subject parameter estimates inversely weighted by their variance estimates. In essence, this is a fixed-effects approach, since it does not take into account between-subject variances. Note that, this is also a summary statistics method.

In conclusion, parameters estimated at subject level are the same for all of these four methods, namely FFX, RFX and MFX and ΨFX. After specifying subject-specific GLMs, one calculates subjects' parameters and variances and continues towards average group activation calculation. Since, we are generally not interested in all of the parameters but rather in a particular linear combination of them, contrast vectors are specified at the subject level and applied to the parameter and variance estimates.

3.1.2 Bayesian Inference

Bayesian analysis of hierarchical GLM has been applied extensively to fMRI signals [41, 42, 48]. Implementation of Bayesian methodology for fNIRS signals will

also follow similar procedures. Noninformative priors were specified as in [48], since no prior information is available and generally the number of subjects is so small to make the influence of the prior significant. The details of the Bayesian analysis are presented in Appendix B. Since the modes of the conditional posterior probability distribution functions can easily be calculated, an algorithm like iterated conditional modes (ICM), [50], can be used. Beginning from some initial values we can cycle through the modes until convergence. ICM was preferred to some other Monte Carlo schemes like Gibbs sampling because of its simplicity and speed, which are important criteria especially for practical purposes. For multimodal distributions ICM has the risk of getting stuck at a local minimum or oscillating, but for unimodal distributions (as it is in this case) ICM gives quick solutions. In actual implementation, the convergence of the algorithm to the same output was checked by starting the chain at different initial points.

The contrast vector was applied only after all of the estimation process has ended and that group parameters were available. As in the classical analysis case, this may be achieved by specifying a contrast vector. The marginal posterior of contrasted group parameters obeys a univariate noncentral Student's t-distribution [51]. We can make inferences using this posterior, and ask whether our contrasted parameter estimates are higher than a particular value.

The main difference between the Bayesian analysis presented here (BPE) and the methods mentioned in the previous section is that the former is not summary statistics. Bayesian analysis, in this implementation, incorporates the group variables into subject parameter estimation process. Hence, all subjects should be analyzed simultaneously, and if a new subject is included in the group, the analysis should be repeated for every subject.

3.2 Experiments

The particular experimental protocol that we used in this study is a variant of Stroop task, which is known to be a good activator for prefrontal cortex [52, 53].

Subjects were asked to perform color-word matching Stroop task whose trials are the Turkish versions of Zysset et al. [54]. Subjects were presented with two words one written above the other. The top one was written in ink-color whereas the bottom one was in white (over a black background). Subjects were asked to judge whether the word written below correctly denotes the color of the upper word or not. If color and word matched, then subjects were to press the left mouse button with their forefinger, and if not, the right mouse button with their middle finger. Subjects were informed to perform the task as quickly and correctly as possible. The words stayed on the screen until the response was given with a maximum time of 3 sec. The screen was blank between the trials.

The experiment consisted of neutral, congruent and incongruent trials. In the neutral condition upper word consisted of four X's (XXXX) in ink-color. In the congruent condition ink-color of the upper word and the word itself were the same, whereas in the incongruent condition they were different.

The trials were presented in a semi-blocked manner. Each block consisted of 6 trials. Inter-stimulus interval within the block was 4.5 seconds and the blocks were placed 20 seconds apart in time. The trial type within a block was homogeneous (but the arrangements of false and correct trials were altering) There were 10 blocks of each type. Experiments were performed in a silent, lightly dimmed room. Words were presented via an LCD screen that was 0.5 m away from the subjects. The task protocol is approved by the Ethics Review Board of Boğaziçi University.

12 healthy (7 female, 5 male) subjects from the university community (right-handed, mean age 26.17 ± 4.30, range $20 - 31$) participated in the study. Subjects had no reported neurological, medical and psychiatric disorders. None were taking medications at the time of measurement. All the subjects had normal or corrected-to-normal vision and normal color vision. Written informed consent was obtained from all subjects before the measurement.

3.3 Results

Stimulus onset vectors for each type of stimulus (neutral, congruent and incongruent) were formed and convolved with the canonical HRF [55]. These three vectors constituted the cognitive part of the design matrix. The fNIRS data were digitally low-pass filtered with a cut-off frequency of 330 mHz. To be able to cope with various low-frequency trends, discrete cosine transform basis functions [56], were added to the design matrix with a minimum period of 120 seconds. Incorrect and omitted trials were modeled separately and they, together with the trend terms, form the nuisance part of the design matrix.

3.3.1 Behavioral Results

Reaction times (RT) were calculated only from the correctly answered trials. Figure 3.1 shows that the first and second subjects responded slower to congruent trials in comparison to incongruent trials. Subject 6 responded slightly slower to neutral trials than congruent trials. For the rest of the subjects the ordering of RTs is neutral-congruent-incongruent. The average RTs to neutral, congruent and incongruent trials are $1029.3 \pm 277.1, 1183.9 \pm 370.5$ and 1308.8 ± 367.1 ms, respectively. Comparing the RTs, two-tailed paired-t test revealed significant differences among all 3 trial types: Incongruent vs. Neutral $t(11) = 7.042$ $p = 0.000$; Incongruent vs. Congruent $t(11) = 2.882$ $p = 0.015$; Congruent vs. Neutral $t(11) = 4.351$ $p = 0.001$.

There are two common effects in Stroop task: First, the interference effect refers to the observation that subjects have more difficulty in answering incongruent trials with respect to neutral trials. Second, facilitation effect comes from the observation that subjects respond quicker to congruent trials compared to neutral trials [57]. Although the interference effect was evident in RTs, we could not observe a facilitation effect. Using the same kind of stimuli Zysset et al., [54], has not observed facilitation effect either. It has been pointed out that facilitation was not a necessary concomitant of interference and it played a much lesser role than interference [52]. It was asserted

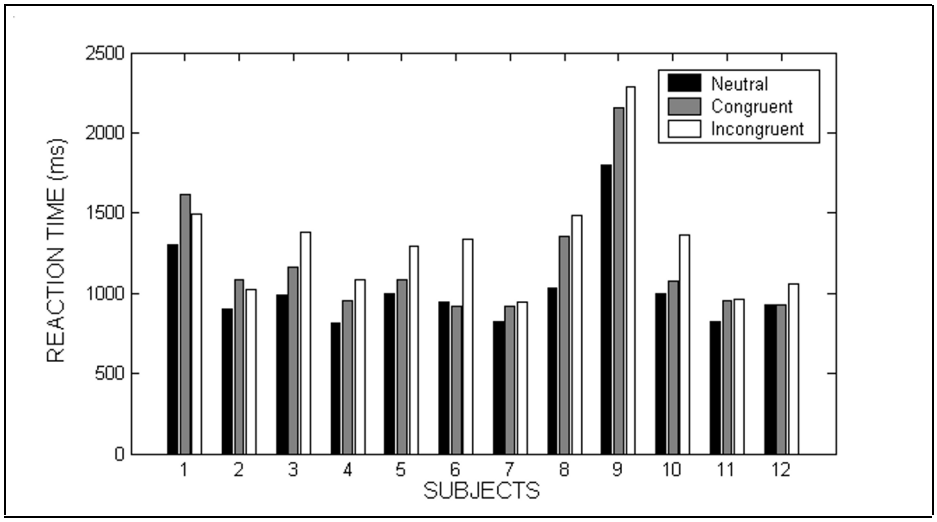

Figure 3.1 Reaction times of the subjects.

that the missing facilitation was due to trying to speed up an already rapid response. Additionally, the slower response to congruent trials may be related with the observation that the subjects try to judge whether the trial is congruent or incongruent, which puts an extra cognitive load with respect to neutral trials.

Error rates were generally small, and most of the subjects did not make any mistakes for neutral and congruent trials. Mean error rates (in percentage) were $0.56 \pm 1.92, 0.56 \pm 1.30$ and 4.31 ± 5.97, respectively for neutral, congruent and incongruent trials. No statistical test was carried out in terms of error rates since they were generally so small; however, it can be said that interference effect also manifests itself in error rates.

3.3.2 fNIRS Results

fNIRS device provides us with a set of time series recorded over 16 channels over the scalp. For the locations of the probed regions refer to Figure 2.3. Note that the ordering of the channels is from left to right, that is, "‘1"’ is on the left and "‘16"’ is on the right. Oxy-Hb and deoxy-Hb data were analyzed separately.

3.3.2.1 Oxy-Hb results. The subject level and group level activation patterns for interference effect (incongruent - neutral) are shown in Figure 3.2. These patterns and the others presented in the following figures result from the thresholded z-scores at 0.05 significance level (that is, $z_{thresh} = 1.65$ and $p = 0.05$, adjusted for multiple comparisons by Bonferroni correction). The posterior probabilities given by the ΨFX and BPE are also converted to z statistics. Recall that subject-level activations are common for FFX, RFX, MFX and ΨFX, and estimated by ordinary least squares (OLS) in a single step, whereas BPE estimates iteratively both subject and group parameters.

The first observation is that there is activation widespread over channels for most of the subjects. Furthermore, all subject activations resemble each other for both OLS and BPE approaches. This is usual and points to the fact that group level variance is higher than subject level variance, which causes the effect of group parameters being weighted down in the estimation of subject level parameters. Despite the apparent similarity between OLS and BPE methods, the consistent activation in channel 4 revealed by BPE is worth noticing. BPE finds that channel 4 is activated for all of the subjects, while this is not the case for single-level GLM. The second important observation is that the percentage of activated subjects per channel indicates that activation is dominantly left lateral (Figure 3.2, middle row). When group level inference is inspected (Figure 3.2, bottom row), this left laterality is especially evident with RFX, MFX and BPE. Channels 1-4 are found to be active, with channel 4 giving the highest z-value and consistency. Thirdly, it can be seen that the wide spread activation at the subject level is carried over to the group level with FFX and ΨFX. This is to be expected because these two methods do not consider the between-subject variance. The consequence is that FFX and ΨFX have higher sensitivity but at the risk of high false positive rates.

It was also investigated whether there was a significant activation difference between incongruent and congruent trials. The behavioral results have shown that there was no facilitation effect, that is, subjects had more difficulty with congruent trials with respect to neutral trials. This also manifested itself in fNIRS findings and the activations both at the subject and group levels are less pronounced this time (there

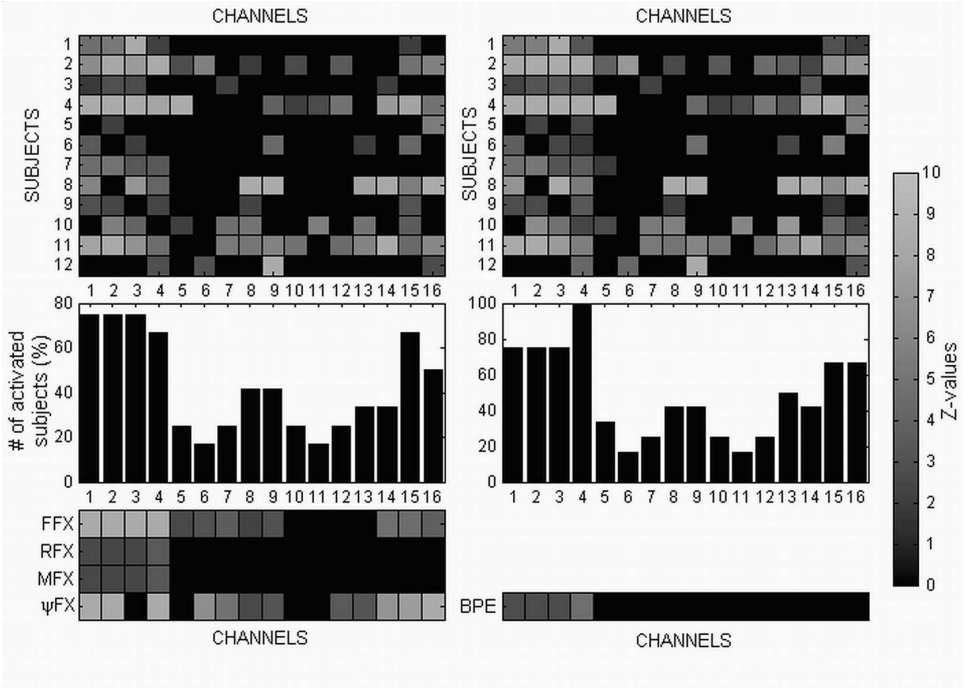

Figure 3.2 Activation patterns for oxy-Hb for "incongruent - neutral" contrast. Top: Subject level activations detected by OLS (left) and BPE (right). Middle: Activated subject count (%) for OLS (left) and BPE (right). Bottom: Group level activations for FFX, RFX, MFX and ΨFX (left) and BPE (right).

is no activated channel for subjects 1 and 6, see Figure 3.3, top row). FFX and ΨFX, again, found higher number of activated channels compared to the other three methods (Figure 3.3, bottom row). The activations of RFX, MFX and BPE are confined to the left lateral channels.

It might be suggested that the medial activations detected by FFX and ΨFX may be due to anterior cingulate cortex (ACC), which has been identified as a region involved in Stroop-like inhibition paradigms [58]. However, it has been shown that ACC is not specifically involved in interference processes, but rather in motor preparation processes [54]. Hence, ACC should not be substantially activated when comparing neutral and incongruent conditions, as the motor response preparation process, once the decision is taken, is the same for both conditions in color-word matching Stroop task [54]. Additionally, considering the penetration depth of near infrared light [59], it is doubtful if fNIRS would be able to capture the activations in ACC with source-detector separation of 2.5 cm. Hence, it may be concluded that the medial activations

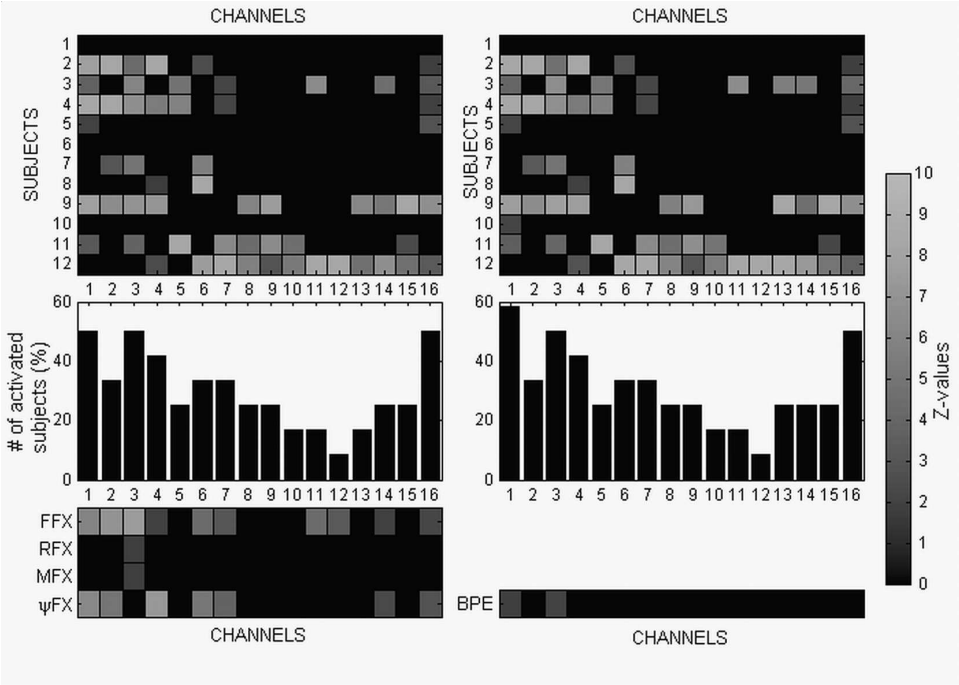

Figure 3.3 Activation patterns for oxy-Hb for "incongruent - congruent" contrast. Top: Subject level activations detected by OLS (left) and BPE (right). Middle: Activated subject count (%) for OLS (left) and BPE (right). Bottom: Group level activations for FFX, RFX, MFX and ΨFX (left) and BPE (right).

detected by FFX and ΨFX are false activations.

Since subjects had more difficulty with answering congruent trials with respect to neutral trials, the group level activation for the difference between these two trial types was also investigated. Although there was some activation at the subject level, no activation could be found at the group level.

It is possible to present the fitted cognitive waveforms to the measured signal as in Figure 3.4. The large slow trend over the signal may be seen in this figure. For the case of this subject, the contrast of 'incongruent vs. neutral' trials is significant while "incongruent vs. congruent" contrast is not.

Up to this point, the main concern was the activation detection problem. In other words, given a canonical HRF signal model it is checked whether there is activation or not in the measurements. The complementary problem would be the estimation

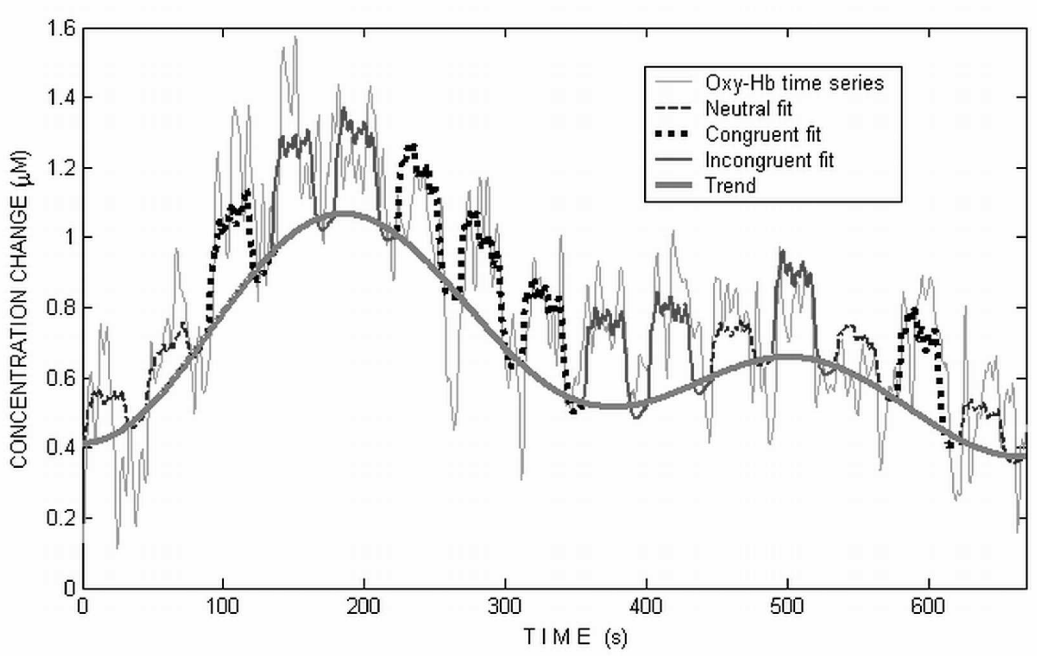

Figure 3.4 An oxy-Hb time series with fitted cognitive waveforms and trend component.

of this HRF signal. To this effect a second GLM was applied where the HRF was modeled as successive time bins, that is, as a finite impulse response filter. In this setting of the problem, the coefficients of the filter should give the HRF waveform. Note that this approach does not put any constraints over the HRF, and effectively, it averages the event-related responses for each subject. Figure 3.5 demonstrates the HRF waveforms for each type of stimulus averaged over subjects. For most of the channels the end result is a plausible HRF waveform. We want to examine especially the waveforms acquired from channels 1-4, since BPE identified channels 1-4 as activated for "incongruent vs. neutral" contrast and channels 1 and 3 for "incongruent vs. congruent" contrast. The resulting waveforms from these channels are also consistent with this result. A caveat is that average waveforms are by no means a direct indication of group activation, but the consistency between the detection and estimation procedures is worth noticing.

3.3.2.2 Deoxy-Hb results. The analysis of deoxy-Hb signals did not discover as strong activation patterns as those of oxy-Hb. Figure 3.6 shows the activations for "incongruent vs. neutral" contrast. In fact, there are activations at the subject level

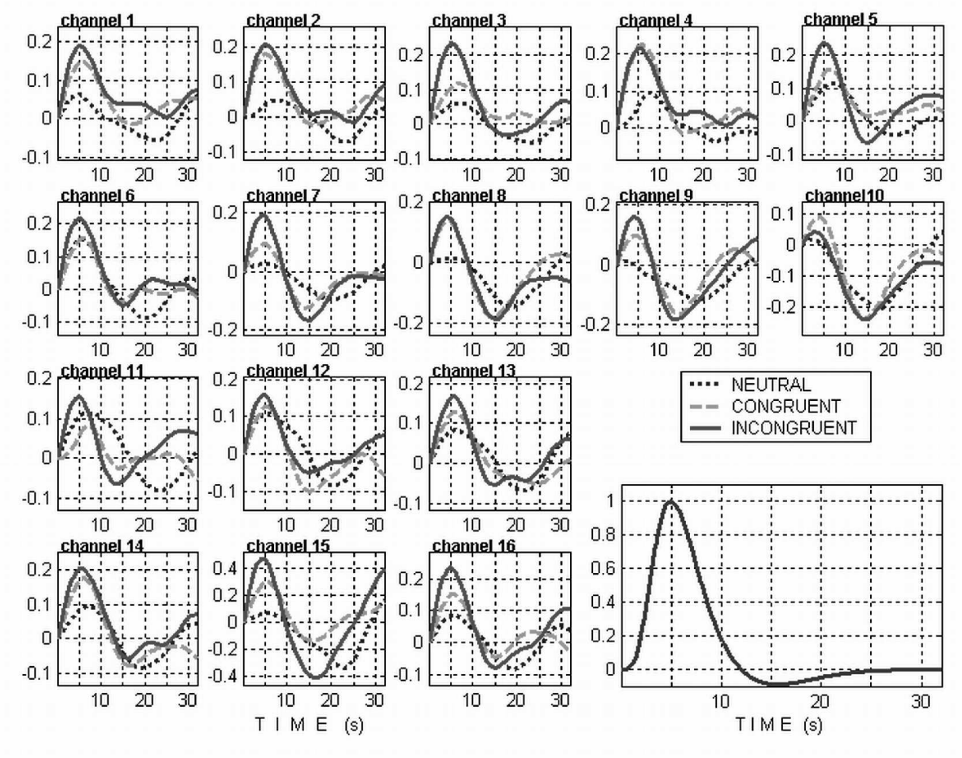

Figure 3.5 Estimated hemodynamic response function waveforms averaged over subjects (running averages over 3 seconds), with hypothetical HRF at the bottom-right.

(Figure 3.6, top row), and these are carried to the group level by FFX and ΨFX; however, RFX, MFX and BPE do not identify any of the channels as significantly activated (Figure 3.6, bottom row). This is a consequence of the fact that deoxy-Hb exhibits a greater variability among the subjects. To demonstrate this variability, consider Figure 3.7. This figure presents the subjects' parameter estimates for the 3^{rd} channel of deoxy-Hb for "incongruent vs. neutral" contrast and again the 3^{rd} channel of oxy-Hb for 'incongruent vs. congruent' contrast. These combinations were chosen because deoxy-Hb shows activation for 7 subjects (out of 12) but with no group activation for RFX, MFX and BPE, whereas oxy-Hb shows activation for 6 subjects along with group activation by the aforementioned methods. The reason for this lies in the greater variance (mainly due to the 1^{st} and 3^{rd} subjects) exhibited by deoxy-Hb. The resulting activations of deoxy-Hb for "incongruent vs. congruent" contrast are presented in Figure 3.8.

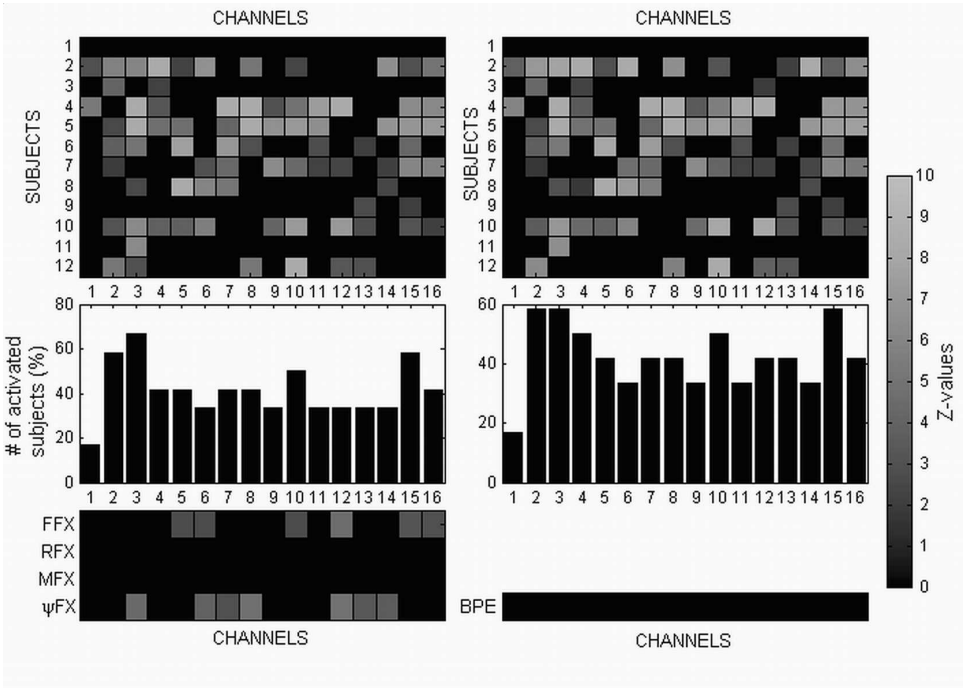

Figure 3.6 Activation patterns for deoxy-Hb for "incongruent - neutral" contrast. Top: Subject level activations detected by OLS (left) and BPE (right). Middle: Activated subject count (%) for OLS (left) and BPE (right). Bottom: Group level activations for FFX, RFX, MFX and ΨFX (left) and BPE (right).

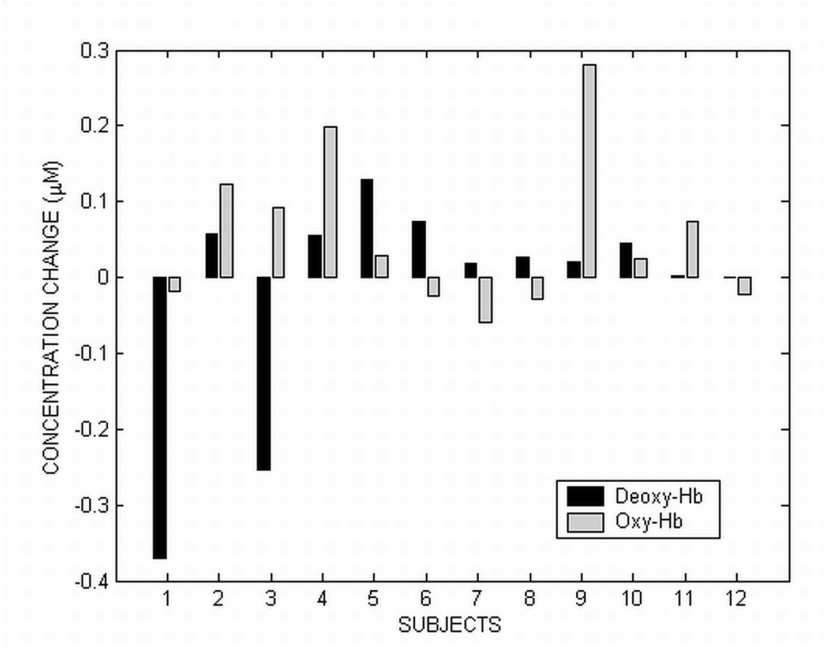

Figure 3.7 An example set of contrasted subject level parameters (see text for detailed explanation).

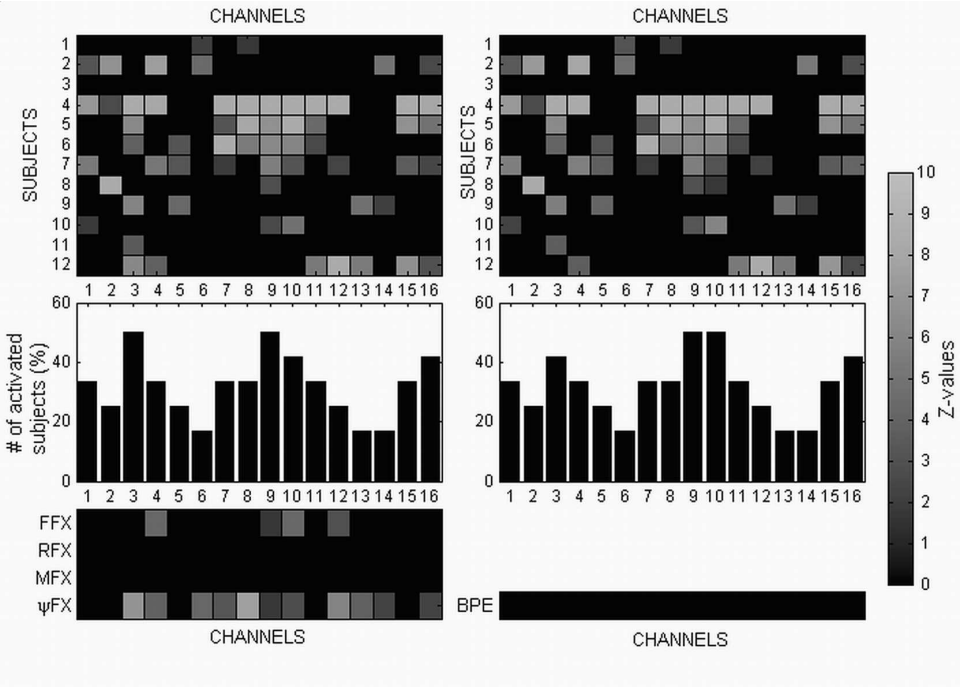

Figure 3.8 Activation patterns for deoxy-Hb for "incongruent - congruent" contrast. Top: Subject level activations detected by OLS (left) and BPE (right). Middle: Activated subject count (%) for OLS (left) and BPE (right). Bottom: Group level activations for FFX, RFX, MFX and FX (left) and BPE (right).

3.3.2.3 Relation between hemodynamic and behavioral responses. The relation between hemodynamic and behavioral responses were investigated by finding the channel-by-channel correlation coefficients between the interference effects measured by the difference in concentration changes and reaction times of incongruent and neutral trials. Significant correlation was found for oxy-Hb in the 4^{th} channel ($r = -0.57$ $p = 0.05$). The 4^{th} channel was the most consistently activated channel across subjects. Scatter plot of behavioral vs. hemodynamic response for this channel is shown in Figure 3.9. Note that, the correlation is negative, i.e., hemodynamic response is smaller for higher behavioral interference effect. This finding supports the hypothesis that "higher Stroop-specific brain activation leads to more successful inhibition of competing responses and hence, a smaller behavioral interference effect" [60]. Not very surprisingly, no significant correlation was found between reaction times and hemodynamic responses for the "incongruent vs. congruent" contrast of oxy-Hb and for both of the contrasts of deoxy-Hb.

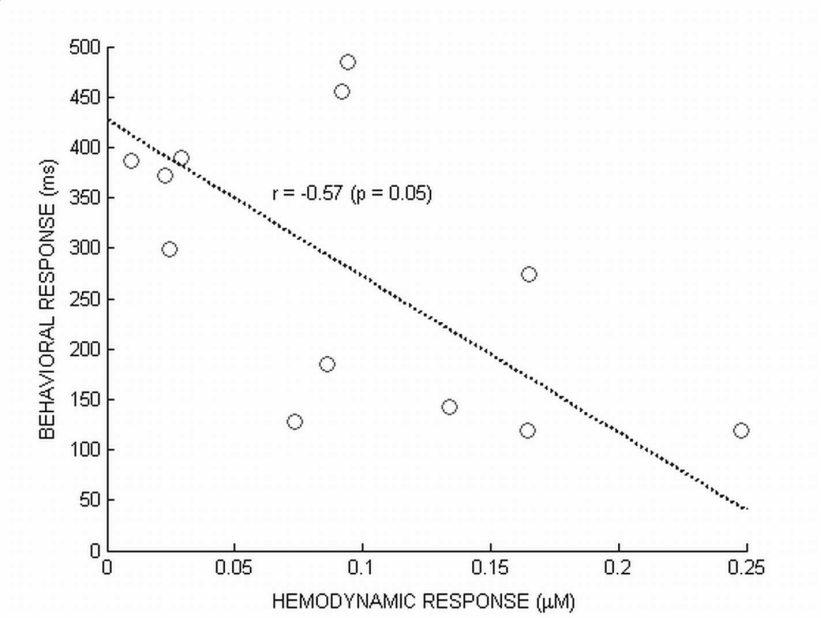

Figure 3.9 Correlation between the hemodynamic and behavioral responses for oxy-Hb in the 4th channel during interference ("incongruent - neutral") condition.

3.4 Discussion

The results corroborate the conjecture that fNIRS data lend itself to multilevel statistical inference. Consistent activation patterns were observed during Stroop interference, particularly for oxy-Hb. It may be recommended that application of multilevel statistical inference to fNIRS data should always include random effects, and MFX or Bayesian methods may be preferred for this purpose. The problem with fixed effects models is that it ignores between subject variability and since within-subject variance is much smaller it becomes possible for the channels to have illusory activation. To overcome this risk, extensions to FFX, like conjunction analysis, may be pursued [61].

Bayesian methodology may have a number of advantages over classical procedures in analyzing multilevel GLMs. First of all, it can cope better with the classical problem of within-subject and between-subject variances in a more principled framework [41]. Bayesian analysis also in this work enabled us to include the information obtained from the rest of the group in the analysis of the particular subject.

Moreover, Bayesian statistics yield posterior distributions for the parameters

of interest. This enriches our statistical test dictionary, which means that we are no longer limited with just NHSTP. Hence we are able to test whether the effect is greater than a meaningful size in relation to the underlying physiology [41]. This is important because the statistical significance obtained by NHSTP in classical statistics does not truly reflect the magnitude of the effect [62]. For example, a very small but consistent effect might be found to be statistically significant. Although, a small but very reliable activation may be interesting, neuroimaging is generally interested in activations of nontrivial magnitude, and this speaks for the usefulness of Bayesian inference. The associated probability, p, of the NHSTP statistic is a conditional probability, $p(data|H_0)$, H_0 being the null hypothesis. If $p(data|H_0)$ is small, this does not necessarily imply that $p(H_0|data)$ is small or that $p(H_1|data)$ is big, H_1 being the alternative hypothesis. Thus, NHSTP does not allow us to ask such questions related with the posterior distribution as "what is the probability that the effect size is bigger than 1?" or "what is the probability that it is 0?" or "does the effect explain 10% of the total energy content of the signal?" This sort of questions become important for fNIRS monitoring of cognitive activity because it is known that, given enough data (in terms of number of time points, subjects etc.) the probability of false activations increases. Thus, it is desired to be able to differentiate trivial departures from the null hypothesis from significant nontrivial effects, and this demands for the probability distribution of the activation given the data. In this respect, classical statistics falls short of proving or disproving activation patterns in a "long" and temporally correlated record of an fNIRS signal.

An interesting point is that using noninformative priors carries the Bayesian inference closer to classical inference. This was also pointed out in [63] in a different context. The rationale for the use of noninformative priors is that cognitive fNIRS studies are at their early stage of development and it would be better not to commit ourselves prematurely; furthermore generally the number of subjects is small so as to make the influence of the prior a lot significant. One of the goals in this study was to compare classical and Bayesian inference methods for fNIRS data. Since classical procedures work with the null hypothesis and ask whether the effect size is greater than zero or not, the same threshold was also assigned for the Bayesian analysis for comparison.

The proposed Bayesian method necessitates the simultaneous analysis of the data of all the subjects'. Thus, if a new subject is added to the group, it is necessary to redo the whole analysis. Obviously this poses a problem for fMRI since in this case there are thousands of voxels, and hence for all of them the analysis must restart from scratch. Although fNIRS also requires redoing all the calculations, the number of detectors is two orders of magnitude less, in fact on the order of tens. Moreover, we make use of a fast iterative scheme, ICM, which substantially reduces the runtime of the algorithm. During the analysis no contrasts were applied in the intermediate levels and all the parameter estimates were passed up to the highest level. This enables us first, to take into account the correlations among the subject level parameter estimates and second, to make the simultaneous testing of a number of hypotheses.

The multiple comparison problem arising from the simultaneous testing of a number of channels was tried to be circumvented by Bonferroni correction. It is known that Bonferroni correction is too conservative, especially when there is spatial correlation between the measurements [64]. A promising method for NIRS signals was put forward using the false discovery rate procedure [65]. However, as also noted in that study, multiple comparison correction of multichannel NIRS studies is still an open problem.

One particular issue that has not been discussed so far is the effect of differential path length factor (DPF). Although in this study it was kept fixed across subjects (DPF = 5.93), it is known that DPF may show variations among subjects [32]. However, it is not possible to estimate the exact DPF for every subject. It was proposed to use DPF-independent measures in the analysis of fNIRS signals and GLM was put forward as a candidate for this task [27]. The reason was that the statistics produced by GLM was independent of the DPF. Relevant to this study is that when we try to combine the parameter estimations from different subjects this DPF dependency will clearly affect the results. Despite this fact, it is possible to reduce this effect substantially by MFX, ΨFX and BPE type of algorithms. In these algorithms the effect of subjects on the group results is inversely proportional to their estimation variances. Hence, this procedure also acts as a normalizing term, and eliminates, in part, the effects of

DPF variations. RFX, on the other hand, directly calculates group variance estimate from the variance of subject parameter estimates. Then, the estimated variance will definitely include both real concentration change variances and also the variations caused by DPF differences.

The Stroop findings are generally consistent with the literature, though they are not as strong and conclusive as those of [66], where they showed activation bilaterally for both oxy-Hb and deoxy-Hb. However, in this study activation was found only for oxy-Hb in the left lateral prefrontal cortex and there was no activation (at the group level) for deoxy-Hb. These results coincide more with those of [67], where they also found only left lateral activation for oxy-Hb and showed that the activations for deoxy-Hb were much weaker. In a comprehensive review, [52], it was concluded that the left hemisphere generally showed more interference than the right. These findings also point to an important aspect of fNIRS data analysis: The consistencies and controversies between the results obtained by oxy-Hb and deoxy-Hb. In [27], using a visual stimulus, it was concluded that deoxy-Hb is more amenable to GLM. However, in another study, [68], it was concluded that cortical activation could lead to different patterns in deoxy-Hb and was proposed oxy-Hb as the best indicator of regional cerebral blood flow changes. There were also other findings supporting this hypothesis [67]. On a reproducibility study of event related fNIRS, it was stated that deoxy-Hb was associated with lower t-values at single subjects' level as well as at the second level if compared to oxy-Hb [69]. In another study on false memory on the prefrontal cortex [4], deoxy-Hb did not show any significant activations and the authors stated that this might be attributable to the instability of deoxy-Hb concentration which was largely determined by the wash-out effect of the regional cerebral blood flow increase [70]. In a simultaneous fMRI-fNIRS study [71], it was found that oxy-Hb was a more robust hemodynamic signal and correlated more with fMRI-BOLD response. This was attributed to the lower signal-to-noise ratio of deoxy-Hb signal. However, in another study [72], using an experimental design that increased the signal-to-noise ratio of NIRS signals, it was found that deoxy-Hb was more correlated with fMRI-BOLD signal. When evaluated together, these findings point to the fact that although oxy-Hb is more dominantly labeled as the carrier of cognitive information, the potential of NIRS for measuring

cognitive activity and the interpretation of deoxy-Hb and oxy-Hb still need further research. The results of this study indicate that oxy-Hb is more sensitive to regional blood flow changes in the prefrontal cortex caused by cognitive stimulus. Consistent left prefrontal activation was found for oxy-Hb during Stroop interference. The activation patterns at the subject level are more structured and the hemodynamic results show a better correlation with the behavioral results for oxy-Hb than deoxy-Hb.

4. GLM ANALYSIS UNDER PARAMETER CONSTRAINTS

One of the most important aspects of GLM analysis is the selection of appropriate waveforms for modeling hemodynamic response function. Canonical HRF (cHRF), which is composed of the difference of two gamma functions, is commonly used for this purpose. Since mismatches between the hypothetical and actual waveforms can substantially decrease the detection performance, some flexibility is allowed in the basic model in order to better capture the variations in the hemodynamic response. Employing temporal and dispersion derivatives (TD and DD) along with the cHRF is one of the most common ways to attain a more robust analysis [55]. Accordingly, the HRF is modeled as a linear combination of three waveforms. However, even if a successful waveform modeling is apparently obtained, there is still a concern about the reliability of the analysis and it should be checked whether it represents a plausible HRF or not. Obviously if there are no restrictions on the linear combination weights, then unrealistic HRFs may be obtained, and consequently activations may be detected when there are none.

Constraining the basis set for modeling the HRF has been studied using variational Bayes where basis waveforms were formed via singular value decomposition of a set of plausible HRF sample waveforms [63]. Then using regression analysis, a multivariate normal distribution was fitted for the basis weights and this information was used as prior distribution in the Bayesian analysis. This was a "soft-constraint" approach in the sense that multivariate normal could not capture all details of the true distribution. Despite this limitation, this work has shown that constraining the basis set allowed for superior separation of active voxels from non-active voxels in fMRI data. The method of constraining the linear combinations of the basis set has also been taken up in the canonical correlation analysis framework [73]. The limitation of this work, however, is that only positivity of the linear combination coefficients is required.

In this chapter, which is based on [74], the problem of doing constrained parameter estimation and inference with GLM is studied in a Bayesian framework. Using the canonical basis set, consisting of the canonical waveform, its temporal derivative and dispersion derivative, an admissible region is defined in the three-dimensional weight space, and Gibbs sampling is used to arrive at posterior distributions. More explicitly, uniform prior distributions are specified for the parameters. The support of these uniform distributions represents our a priori knowledge, and thus we are sure that the parameter estimates belong to the feasible set. Since, a new basis set is not introduced and the canonical basis set is used, the method is a direct extension of the commonly used GLM for neuroimaging.

The research for the temporal dynamics of HRF is generally based on fMRI. There are numerous studies where functional magnetic resonance imaging and near infrared spectroscopy data are simultaneously acquired and the estimated hemodynamic responses are compared [72, 75]. Although there is a commonly accepted canonical HRF waveform, the instantiations of observed effects can differ in terms of rise time, undershoot, delay, duration etc. The constrained HRF estimation may be expected to be more effective for NIRS analysis, on the one hand, by allowing controlled variations around a canonical HRF that was tailored for fMRI, and on the other hand by leading to a better assessment of the cognitive activity via fNIRS. In summary, constraining the GLM may enable us to be flexible enough to cope with variations in the HRF waveform, but also stringent enough not to allow unrealistic HRF shapes.

4.1 Constraining the Basis Set

The canonical basis set is reproduced in Figure 4.1a, where the peak values of the waveforms are scaled to unity. Sample HRF waveforms were generated by varying the coefficients of the two derivative terms in linear combinations. The resulting waveforms were tested for their plausibility and a tally of the coefficients that satisfied these criteria was kept. An HRF is shown in Figure 4.1b with the parameters that characterize its main features. The setting of parameter ranges was based on information gleaned

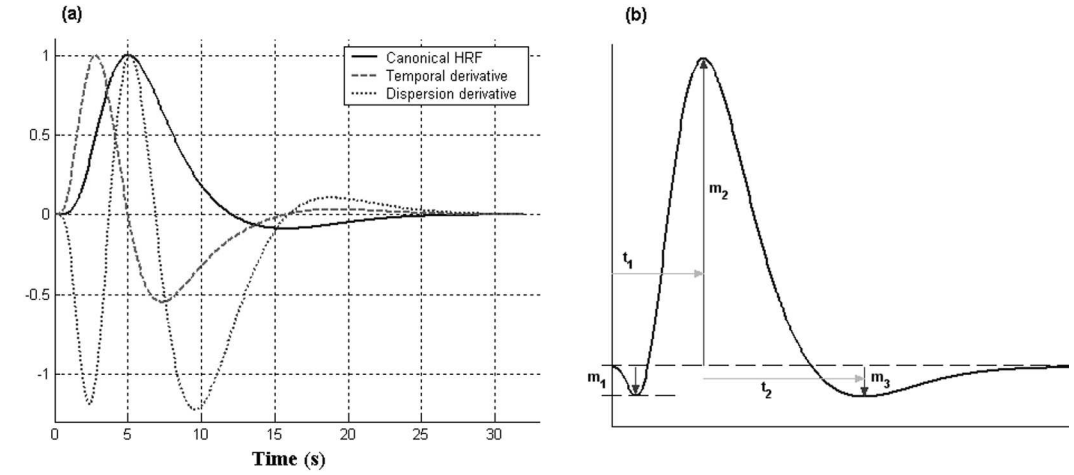

Figure 4.1 a) Canonical HRF with its temporal and dispersion derivatives (maximum value scaled to unity), b) Parameters that characterize the HRF: t_1: Time to peak, t_2: Time to undershoot from peak instant, m_1: Magnitude of initial dip, m_2: Magnitude of main response, m_3: Magnitude of undershoot.

from the literature on temporal dynamics of the HRF [76, 77, 78] and the work on constrained basis sets [63]. An alternative might be using a physiological model, like the balloon model [70], and obtain sample HRFs from this model. The criteria used in determining the plausible HRF waveforms can be listed as,

- A main response with a peri-stimulus time of $3-8$ seconds: $3 \leq t_1 \leq 8$,
- More than one positive peak,
- No more than two negative dips,
- An initial dip with magnitude not greater than quarter of the magnitude of the onset: $0 \leq m_1 \leq m_2/4$,
- An undershoot after $2-8$ seconds after the main peak: $2 \leq t_2 \leq 8$,
- Magnitude of the undershoot not greater than half of the magnitude of the onset: $0 \leq m_3 \leq m_2/2$.

Figure 4.2a shows the feasible region of coefficients of the temporal derivative (TD) and that of the dispersion derivative (DD). The nonrectangular shape of the

feasible region indicates that TD and DD coefficients are statistically dependent. Figure 4.2b shows the plausible HRF waveforms obtained by sampling the permissible TD-DD region.

Since the activation is defined as an increase of oxy-Hb and a decrease of deoxy-Hb, the coefficient of the cHRF is expected to be positive. The NIRS device measures the concentration value in molar units, and the coefficient of the cHRF is constrained to be between 0 and 5 micro molar. This range is broader than typical cognitive activation magnitudes in the prefrontal cortex found in several NIRS studies [79, 80]. For deoxy-Hb, the time-series can be inverted in sign and the same constraints can be applied. The constraints on these 3 parameters then define a volume in 3-d space.

4.1.1 Bayesian Analysis of the Constrained GLM

GLM is formulated in the same manner as the subject-level GLM of the previous chapter, and its details are given in Appendix A. As a reiteration, $Y = Xb + Zh + e$, describes the basic GLM, where Y is the N-sample vector of NIRS data (oxy-Hb or deoxy-Hb), X is the $N \times p$ design matrix, b is the p vector of parameters for effects of interest, Z is the $N \times q$ matrix modeling the nuisance effects, h is the q vector of parameters for nuisance effects, and e is the N-long noise vector. Y, X and Z are known and b, h and e are unknown. In the Bayesian analysis of the GLM, priors are specified for the unknown variables and posterior distributions are derived. The constraints for b, effectively the priors of b, have already been defined in the previous section. To complete the Bayesian analysis we have to specify priors for h and e. Since we have no prior information about nuisance effects, their prior will be set to uniform distribution: $p(h)\ \alpha\ uniform$. The noise is assumed to be uncorrelated, zero-mean, Gaussian distributed with variance σ^2, for which the Jeffreys (noninformative) prior is used: $p(\sigma^2)\ \alpha\ \sigma^{-2}$. Using Bayes rule, full conditional posterior distributions for the variables are found so that Gibbs sampling can be used to generate sample values from the posterior. At each sampling instance, the feasible intervals for the elements of the b vector are imposed. Note that the posterior of the b vector is just

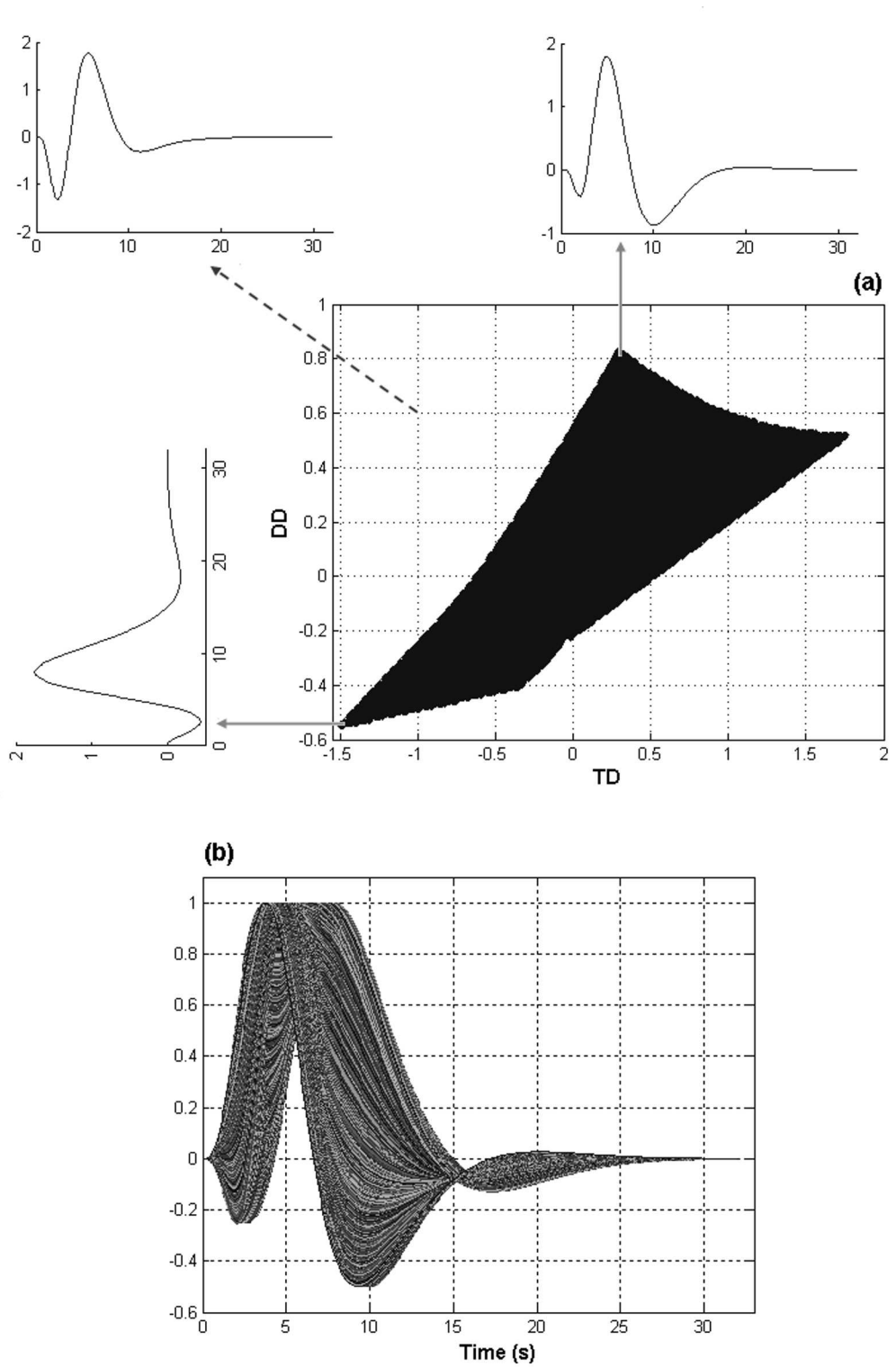

Figure 4.2 a) Feasible values for the coefficients of the derivative terms. Straight arrows indicate two instances of admissible waveforms and dashed arrow indicates a non-admissible waveform, b) The set of plausible HRF waveforms (maximum values scaled to unity).

the truncated version of the likelihood, since $p(b/Y) = p(Y/b)p(b)$, and $p(b)$ acts like a range delimiter. We can use the technique introduced in [81] to draw samples from this truncated distribution: If F_i is the likelihood function for b_i, and U is a uniform $(0, 1)$ variate, then $\hat{b}_i = F_i^{-1}\left[F_i(a) + U(F_i(b) - F_i(a))\right]$ is a random variate from the truncated likelihood (posterior), where the feasible interval for b_i is $[ab]$. The execution of the Gibbs sampling can be summarized as below:

1. From $i = 1 : p$, sample b_i from $p(b_i|b_{-i}, h, \sigma^2)$, where by convention b_{-i} denotes all the b parameters except the i^{th} one,
2. Sample h from $p(h|b, \sigma^2)$,
3. Sample σ^2, from $p(\sigma^2|b, h)$.

Since we are assuming additive Gaussian noise, the likelihood function also has a Gaussian form. Hence, the distribution in the first step is a truncated univariate Gaussian; the distribution in the second step is a multivariate Gaussian and in the last step it is inverse Gamma distributed. After obtaining the posterior distribution of the parameters given the observations, we can use these posteriors to make inferences about the parameters and the related events. In the execution of Gibbs sampling, the chain was run for 10.000 iterations and the first 2.000 iterations were discarded as burn-in. Then, the marginal posterior distribution can be obtained by smoothing the sample-based histogram with a Gaussian kernel.

4.2 Experiments

NIRS data were recorded from 15 volunteers (8 male, age 26.5 ± 4.7 years) recruited from the university community. Subjects had no reported neurological, medical and psychiatric disorders. None were taking medications at the time of measurement. Written informed consent was obtained from all subjects before the measurement. Data

were obtained from the prefrontal cortex of the subjects during color-word matching Stroop task [54], whose details are given in the previous chapter.

4.3 Results

To put into evidence the role of constrained GLM vis-à-vis unconstrained GLM two sets of experiments were ran. These two approaches are denoted, respectively in a more suggestive way, as the Bayesian approach and the non-Bayesian or frequentiest approach. In the first experiment, the algorithm was applied on null hypothesis data, where we expect the Bayesian approach to yield low significance values while the frequentiest approach strives to model events even where there are none. Conversely, the Bayesian approach is expected to yield higher reliability scores on the alternative hypothesis data, that is, when there is an event. In classical analysis, the effect sizes for different contrasts are tested against zero. Since in the constrained analysis the coefficient of the cHRF has already been restricted to be positive, a difference contrast should be used. On the other hand, since Bayesian analysis gives us posterior distributions, it is possible to define a threshold other than zero, and make inference even in one stimulus case. In these experiments with artificial and real data, experimental paradigms with more than one stimulus were used. Inference for activation was based on the main component (cHRF) while the two derivative terms (TD and DD) modeled the variations in the basic HRF, that is, the associated t statistic was produced for cHRF to test the activation. An alternative might be to investigate the total power explained by the linear combination of the basis functions with an F statistic. However, it it known that F statistic is always less sensitive and t statistic based on the cHRF is recommended, especially when the shift in the HRF is known to be less than 1 second [82].

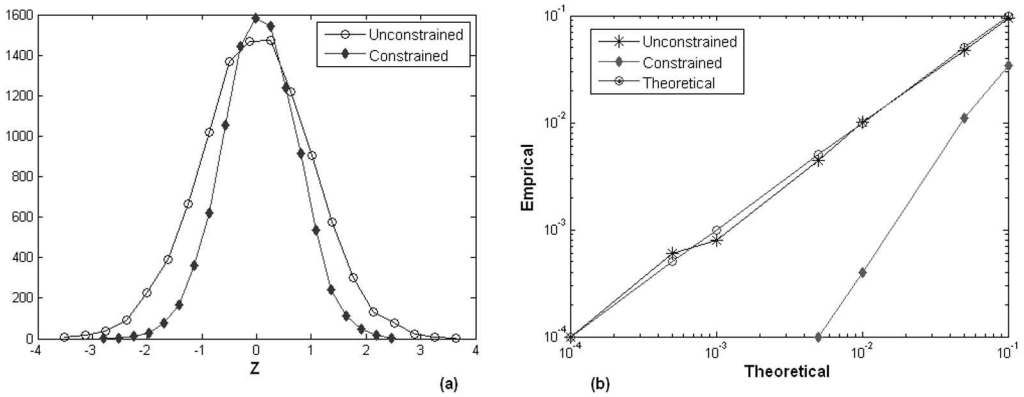

Figure 4.3 a) Histograms of the z-statistics for the unconstrained and constrained analysis from artificial null data, b) Log probability - Log probability plots for the tail masses of theoretical and empirical (constrained and unconstrained) cases.

4.3.1 Artificial null data

10.000 artificial null data were generated using Gaussian noise and a number of trend terms simulating the background activity. A thought-experiment was designed with two stimuli in an event related setting with inter stimulus interval of 20 seconds. Forming a design matrix using cHRF, its derivatives and discrete cosine transform functions for modeling the linear trends (nuisance part), the parameters were estimated using both unconstrained OLS and constrained Bayesian analysis. Finally, the z-statistics of the contrast between the cHRF parameter values of the two stimuli were calculated. The z-statistics (or *pseudo-z-statistics* [63]) were obtained from the marginal posterior for the constrained case Figure 4.3a shows the histogram of z-statistics obtained for the artificial null data for the two analysis cases. It can be observed that the z-histogram is more concentrated around 0 for the constrained case. The reason is that constraining the basis set penalizes the unlikely parameter values and lowers their significance. The log-log probability plot in Figure 4.3b shows the probabilities under the tail for a given z-statistic for both frequentiest (unconstrained) and Bayesian (constrained) analysis. It may be observed that the empirical frequentiest probabilities are in conformance with the theoretical probability values, that is, the z-scores one would obtain in pure noise, whereas the Bayesian analysis produces much smaller probabilities. This means that constraining the basis set reduces false activations.

4.3.2 fNIRS data

Reaction times for the neutral, congruent and incongruent trials were 1028.9 ± 193.2, 1160.6 ± 265.6 and 1260.9 ± 242.1 ms, while the error rates were 0.22 ± 0.86, 1.33 ± 2.11 and 4.00 ± 4.58, respectively. Since error rates were small, the interference effect (incongruent - neutral) was calculated only in terms of reaction times. There was a clear interference effect with $p < 0.0001$. The difference between the reaction times of incongruent and congruent trials and congruent and neutral trials were also significant ($p < 0.01$).

Since interference effect is known to be well pronounced in Stroop task [52], which has also manifested itself in the behavioral analysis, it was decided to concentrate on this contrast for hemodynamic response results. Although NIRS can measure both oxygenated and deoxygenated hemoglobin, only oxygenated hemoglobin was used, since the results of the previous chapter showed that oxygenated hemoglobin was a more sensitive indicator of cognitive activity in the prefrontal cortex during Stroop task.

In the GLM to analyze NIRS data, the design matrix (X) consisted of the cHRF and its derivatives convolved with the stimulus onset vectors for each type of trial. The design matrix modeling the nuisance effects (Z) consisted of discrete cosine transform functions to cope with various low-frequency trends. Incorrect and omitted trials were modeled separately and included in the design matrix as nuisance effects. In other words, inference was based on only correct trials. Each channel of each subject was analyzed individually.

Figure 4.4 shows the histogram of z-statistics for the unconstrained and constrained cases for the overall data, 15 (*subjects*) $\times$ 16 (*channels*), for the interference effect. It may be observed that, as it was the case with the artificial null data, histogram is denser for low z values (-2 to 2) under constrained estimation. The reason is that constrained linear combinations preclude unlikely parameter occurrences. At the same time, the constrained histogram has higher absolute z-values at both ends, since in the case of strong activations and deactivations that satisfy the constraints, our

method yields lower variance estimates, which in turn causes the significance scores to increase. Figure 4.5 shows the activation matrix for OLS and Bayesian analysis. One can observe that the constrained analysis results in some deleted activation cells while new activations are added. For instance, while frequentiest inference does not result in any activation for the 11^{th} subject, constrained analysis identifies three active channels at the left lateral cortex. Figure 4.6 explains the reason for this phenomenon. The recording shown is from the 4^{th} channel of the 11^{th} subject. In Figure 4.6a the fitted waveforms with the unconstrained and constrained approaches are superimposed. The actual NIRS recording is very noisy and there is a continuous oscillation that hides the activation. In the unconstrained case, the OLS estimate tries to fit the model to these oscillations by increasing the derivative terms and suppressing the canonical HRF. On the other hand, constrained estimate is not allowed to increase the derivative terms without limit and finds the best fit that satisfies the constraints. The result is that, it models the variations in the basic HRF shape, but does not model the spurious oscillations and reveals the activation that OLS was not able to identify. Note that we are testing for the contrast "incongruent - neutral". Although the difference between unconstrained and constrained cases seems to be more evident for congruent blocks, there is a subtle difference for incongruent blocks. The coefficients estimated for the canonical HRF, temporal derivative and dispersion derivative by unconstrained analysis for incongruent trials are *0.079, 0.436 and 0.163*, respectively. The same coefficients are estimated as *0.228, 0.294 and 0.085* by the constrained analysis. Figure 4.6b shows the HRF waveforms generated by these coefficients. Note that the main response is similar and hence there seems to be only a minor difference between the two cases in Figure 4.6a. However, the unconstrained analysis produces an implausible HRF with the coefficient of the cHRF being very small, whereas constrained analysis captures the same main response with cHRF and cannot increase derivative terms to make the waveform implausible. Consequently, the tested contrast becomes significant for constrained analysis. Hence, constraining the GLM improves the estimates in two opposite directions: It eliminates the activations due to non-sensible HRF waveforms and it brings forth activations that would otherwise remain hidden.

Figure 4.7 shows the HRF waveforms of incongruent trials obtained from the

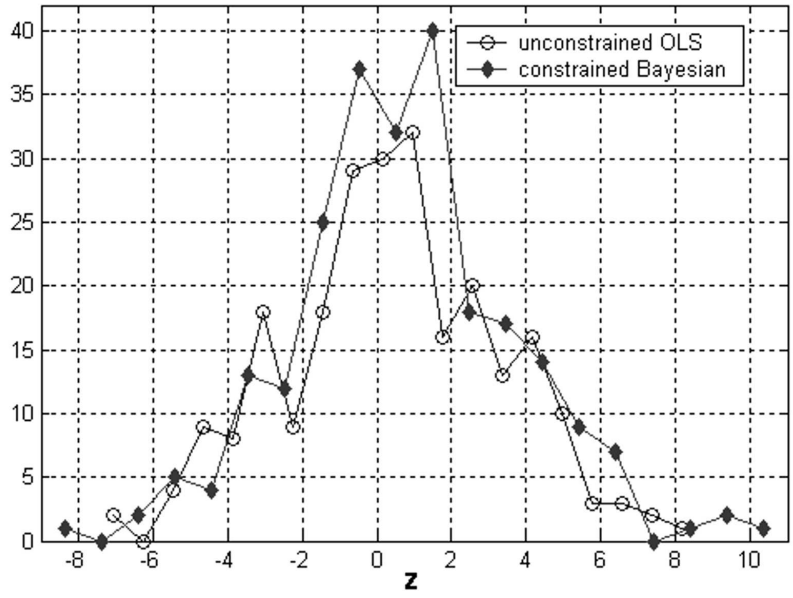

Figure 4.4 Histograms of the z-statistics for the unconstrained and constrained analysis of NIRS data.

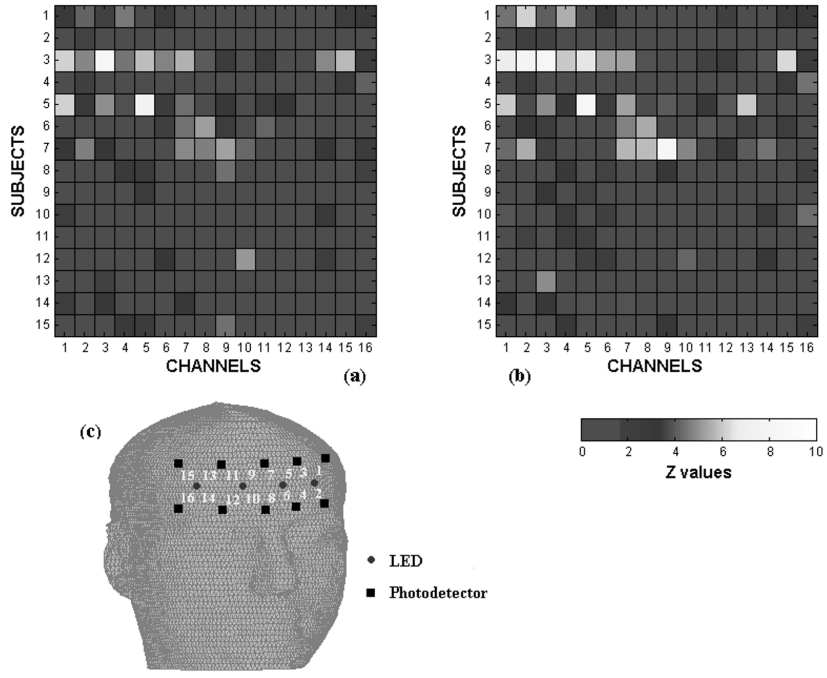

Figure 4.5 Activation matrix (*subjects* × *channels*) thresholded at $p = 0.05$ ($z = 1.65$), for (a) unconstrained, (b) constrained analysis; (c) Placement of the LEDs and photodetectors; channel locations are depicted with numbers.

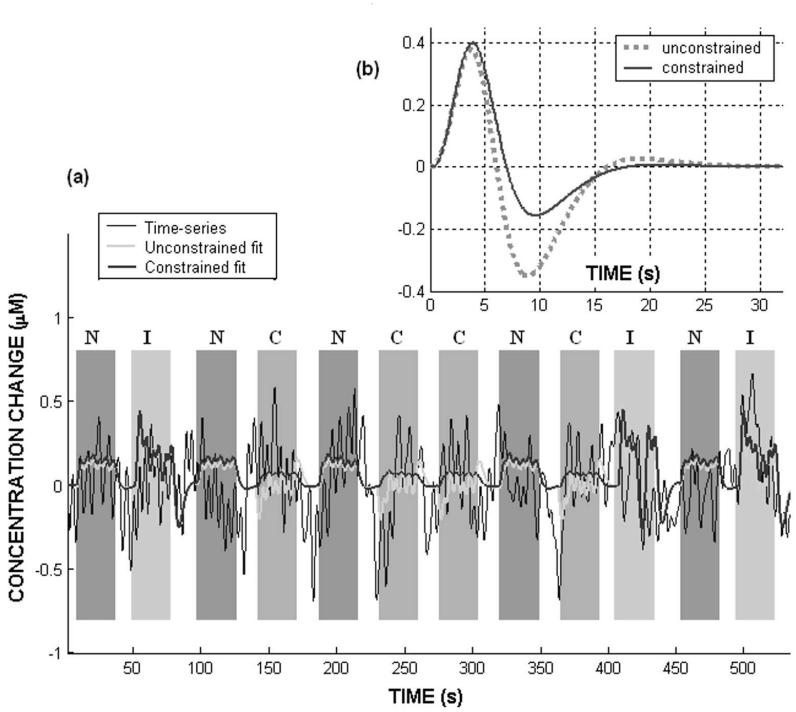

Figure 4.6 (a) Fitted waveforms to a noisy NIRS signal under constrained and unconstrained analyses (N: Neutral, C: Congruent, I: Incongruent trial blocks) (b) Estimated HRF waveforms for incongruent stimulus.

activated channels by constrained and unconstrained analysis. It may be seen that most of the waveforms remain unchanged but the unrealistic HRF shapes are eliminated.

4.4 Discussion

The method presented in this chapter is a direct extension of the classical GLM analysis with the main difference being the constraints put on the solution space to ensure that the resulting HRF is physiologically plausible. The Bayesian methodology enters into the play to constrain the estimation of the parameter vector. It should be emphasized that the proposed approach does not overlook the importance of the exploratory methods. Nevertheless, as the name implies, GLM is a model-based approach and constraining the solution space is a way to ensure that this model really holds.

In another seminal work [63], a method for constraining the linear combination

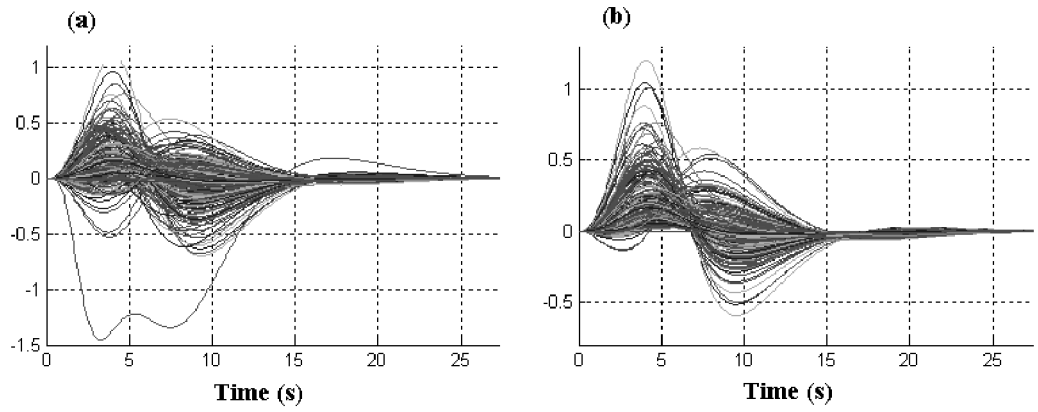

Figure 4.7 HRF waveforms of the incongruent trial for the activated channels obtained by (a) unconstrained and (b) constrained analysis.

of basis sets using variational Bayes was introduced. In that work, a set of plausible HRF waveforms were generated and the basis set that best spanned these waveforms was found. In contrast, rather than developing a new model, an "option" is proposed for classical GLM analysis. In other words, the basis set was considered as given and then all the plausible HRF waveforms that might be generated with it were found. Consequently, a "hard-constraint" approach was adopted in the sense that the prior for the parameter vector is specified as a range-limiting uniform distribution. In the Bayesian analysis uniform prior distributions or indicator functions give rise to truncated posterior distributions, and the latter can be easily inferred upon by Gibbs sampling [83, 84, 85]. In this chapter a simple method was employed to generate samples from a truncated distribution in univariate cross sections [81]. This allowed us, no matter how complicated the constrained space is, to implement the Gibbs sampler after specifying the full conditional posterior distributions of the parameters [83]. Another implementation of sampling from a truncated distribution is to ignore the constraints until the end and then use only the values that satisfy the constraints [51]. However, this scheme becomes very inefficient when the dimensionality of the parameter space is large.

The whiteness assumption about the noise vector is certainly a simplification. In a recent study [86], the severity of the effects of non-white noise on the inference from fMRI signals was reiterated. The characteristics of the noise in fMRI signals is

well-studied and a number of models have been proposed, the most widely used being the autoregressive one [87, 88]. However, the noise in fNIRS signals has not been investigated in detail, yet. It may be conjectured that the models proposed for fMRI may also be valid for fNIRS. However, within this thesis study we assumed that noise vector is white and leave the investigation of its characteristics as a future work.

The criteria proposed for constraining the HRF are by no means complete. The constrained space was tried to keep as flexible as possible but also to respect the main findings of the related theoretical and experimental studies. In summary, a general method is proposed to use the domain knowledge in the form of parameter constraints and incorporate them into the GLM analysis. These criteria can obviously be adjusted as our knowledge on HRF dynamics improves.

5. COMPLEXITY ANALYSIS OF fNIRS SIGNALS

The previous chapters investigate the problem of discriminating signal from noise in a hypothesis-based setting. The significance of some predefinite temporal components were determined using classical and Bayesian techniques. Although this approach stands close to human perception and produces well interpretable results, it is not the only way to search for some patterns in a multivariate time-series data. Amongst the others, information theoretic complexity estimation methods provide summary information in the form of quantitative measures. A complexity defition was put forward for the brain based on its two intervening properties. Neural complexity (C_N) was introduced to reflect the interplay between the functional segregation and integration within complex dynamical systems, of which neural system is an interesting particular case [89]. In this model, (C_N) is low for systems whose components are characterized either by total independence or total dependence, and high for systems which exhibit both specialization and integration. Specialization implies here local organization of a neural system to accomplish one or more sub-task.

The idea of positioning complexity between the two extremes was also advocated by other researchers [90, 91]. Excess entropy was proposed to measure the amount of apparent randomness at small blocks that is explained away by considering correlations over larger and larger blocks [92]. As will be evident in the following paragraphs this is the same mechanism used for calculating C_N. An interesting case is the passage from 1-dimension to higher dimensions. Since in 1-dimension there is a natural ordering of elements, the calculations of entropy and complexity are rather straightforward. However, in higher dimensions there is no natural ordering of elements and the way that these elements are brought together also projects additional spurious structure onto the configuration. This problem was studied using multidimensional templates moving over the data and it was shown that excess entropy is capable of catching structures in dimensions more than one [92, 93]. Although not formulated explicitly, C_N proposes a different way to cope with the problems introduced with multidimensional

data. C_N considers all possible parsings of the data and calculates the complexity for each case and takes the average.

C_N was applied to functional magnetic resonance imaging (fMRI) data obtained during photic simulation of healthy subjects. In this case fMRI measurements from within the brain showed greater complexity from the same data but sampled outside the brain [94]. It was also predicted that C_N would be reduced in neurological disorders where consciousness is reduced. However, testing this conjecture on electroencephalography (EEG) data from generalized seizures and postanoxic encephalopathy, it was found that C_N of the patients was actually higher than the controls [95]. In another study with EEG signals, neural complexity during a visual oddball task has been shown to correlate with subject's cognitive state in a way that depends on the stimulus context [96]. Neural complexity measure was also applied to magnetoencephalography (MEG) data in Alzheimer's disease, and it was found that neural complexity did not decrease in patients, but that there were differences in the frequency bands between controls and Alzheimer subjects [97]. When evaluated together, the findings of these works suggest that although neural complexity is correlated with cognitive activity of the brain, this relationship may not manifest itself always consistently. A topographical approach to neural clustering for understanding, in a more intuitive way, the complexity of a graph has also been proposed [98].

This scheme for studying the neuroanatomical organization of the brain has later been extended with the introduction of "functional clustering" [99, 100]. A functional cluster in the brain can be defined as a set of neural elements that are strongly interactive among themselves, but weakly interactive with the rest of the system. A study with EEG using photic and auditory stimuli showed the existence and different patterns of functional clusters between normal controls and schizophrenics [101]. In another study with EEG during viewing a random dot stereogram, it was observed that brains of the normal controls exhibited greater complexity when they perceived a 3D object than when they did not, and such perceptions also gave rise to a well-defined clustering pattern [102].

5.1 Calculation of neural complexity, C_N

C_N was introduced as a tool to solve the long-lasting controversy between the localizationist and holist views of the brain [89]. C_N is intended to estimate complexity in the sense of information shared among parts of a system and to elucidate the functional segregation and integration within a unified framework. These two aspects of a system are characterized by deviations from statistical independence among its components, which are measured by entropy and mutual information. Accordingly, highly irregular or highly regular systems will show low values of complexity whereas systems with both segregation and integration will have large values of complexity.

For a system Θ with n elementary components, mutual information (MI) between the j^th subset consisting of k elements (Θ_j^k) and its complement $(\Theta - \Theta_j^k)$ is,

$$MI\left(\Theta_j^k; \Theta - \Theta_j^k\right) = H\left(\Theta_j^k\right) + H\left(\Theta - \Theta_j^k\right) - H\left(\Theta\right), \tag{5.1}$$

where $H\left(.\right)$ denotes entropy of the system. Integration is the generalization of the concept of mutual information to multivariate case. Integration of the system Θ, denoted as $I\left(\Theta\right)$, is defined as the difference between the sum of the entropies of all individual components $\{\theta_i\}$ considered independently and entropy of the system Θ considered as a whole:

$$I\left(\Theta\right) = \sum_{i=1}^{n} H\left(\theta_i\right) - H\left(\Theta\right). \tag{5.2}$$

If subsets, Θ^k, composed of *k-out of-n* components are considered, the average integration for these subsets may be denoted as $\langle I\left(\Theta_j^k\right)\rangle$, where the average is taken over all $n!/n!\left(n-k\right)!$ combinations of k components. Consequently, the complexity $C_N\left(\Theta\right)$ of a system Θ is defined as the difference between the values of $\langle I\left(\Theta_j^k\right)\rangle$ expected from a linear increase for increasing subset size k and the actual discrete values observed (see Figure 5.1):

$$C_N\left(\Theta\right) = \sum_{i=1:n} \left[\frac{(k-1)}{(n-1)} I\left(\Theta\right) - \langle I\left(\Theta_j^k\right)\rangle\right]. \tag{5.3}$$

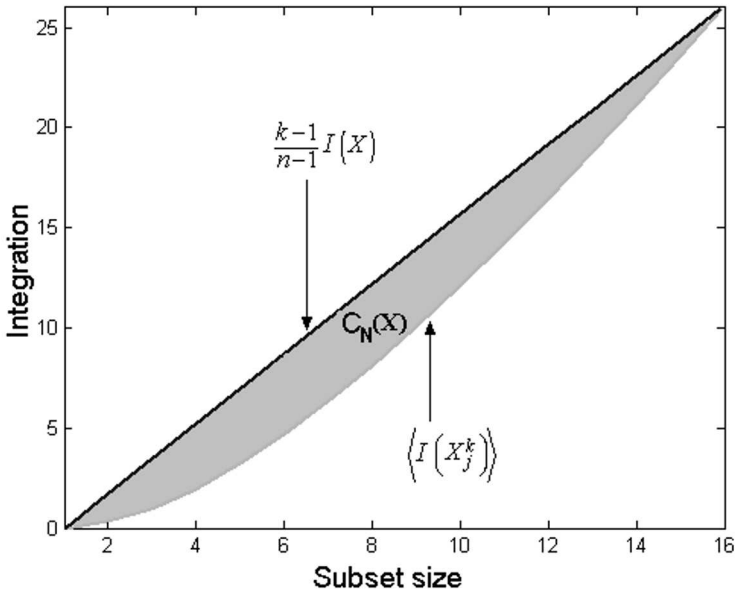

Figure 5.1 Calculation of neural complexity.

Assuming a multivariate normal distribution integration can be calculated by,

$$I(\Theta) = -ln\left|CORR(\Theta)\right|, \tag{5.4}$$

where $CORR(\Theta)$ is the determinant of the correlation matrix.

5.2 Determination of functional clusters

A functional cluster is a group of units which are more interactive among themselves than with the rest of the system (see Figure 5.2). It can be defined as the ratio of the integration of the cluster to the mutual information between that cluster and the rest of the system [99]:

$$CI\left(\Theta_j^k\right) = \frac{I\left(\Theta_j^k\right)}{MI\left(\Theta_j^k; \Theta - \Theta_j^k\right)}, \tag{5.5}$$

where CI stands for the cluster index. A cluster merits to be a functional one only if its cluster index is greater than 1. Since CI is an extensive quantity, that is it grows monotonically with cluster size, one should normalize it for comparing the significance of clusters of different size. This normalization can be achieved by generating random

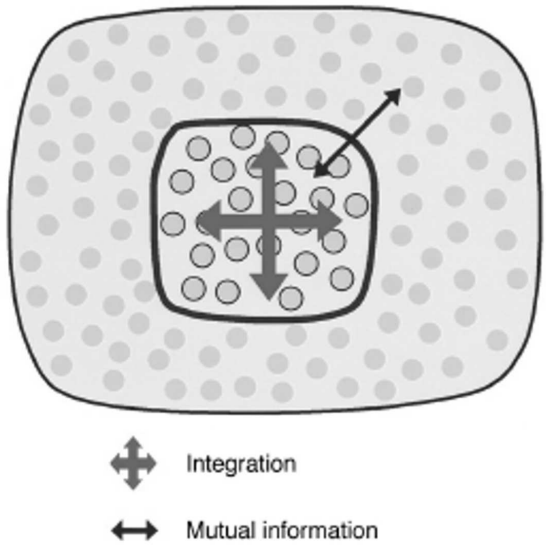

Figure 5.2 Illustration of functional clustering (image obtained from [100]).

samples with the same cluster size and overall integration but not containing any functional clusters. Then, a Student's t-like statistic may be calculated by subtracting the mean *CI* of these random samples from the *CI* of the original data and dividing by the standard deviation of the *CI* of the random samples. 1000 random samples were used in this study and the significance threshold was determined as 0.05. In order to interpret the pattern of functional clustering using the procedure described in [102], for each detector the proportion of significant clusters that they were included in was calculated. Hence, a value between 0 and 1, showing the "probability" of that detector being a member of a functional cluster, was obtained. This procedure was applied to each subject and a mean probability value was derived for each detector position.

5.3 Experiments

To evaluate the performance of the information theoretic complexity measures for fNIRS, data were collected from a group of subjects while doing mental arithmetic (MA) task. MA was used as a stress inducing (negative emotion) task in several studies [103]. Relationship between the asymmetry of the prefrontal cortex activity and heart rate (HR) during MA task has been investigated by near infrared spectroscopy

(NIRS) [104]. NIRS demonstrated increases of oxy-Hb and total hemoglobin (total-Hb) associated with decreases of deoxy-Hb in the bilateral prefrontal cortices. Moreover, the prefrontal hemodynamic activity in the high-HR group was predominantly right-lateralized whereas in the low-HR group the activity was dominated by the left hemisphere. The idea of searching for relations between brain activity and HR stems from the fact that several cortical areas are recognized as the regulators of cardiac performance [105]. At the level of cerebral cortex, it has been shown that HR increase was predominantly accomplished by right-hemispheric activity [106]. This is the consequence of the fact that sympathetic control which causes the acceleration of the heart depends more on right hemispheric influences [107]. The research on hemisphere asymmetry, on the other hand, has suggested that relatively greater left frontal activity is associated with positive effect, whereas greater right frontal activity is associated with negative effect [108]. Although the hypothesis that right hemisphere's influence on the sympathetic control is secondary to hemisphere differences in emotional functions has been objected [107], the results of the past research may be summed up as tasks causing negative emotions should be related with right frontal cortex activation and should cause an increase in the HR.

The experimental protocol was similar to the one used in [104]. The experiment begins with 60 seconds rest followed by 60 seconds of task period during which subjects are asked to subtract a 2-digit number from a 4-digit number as quickly as possible (self paced). After a recovery period of 90 seconds subjects perform a second task period again lasting 60 seconds. The experiment ends with a 60 seconds recovery period.

NIRS data were obtained from 14 high school students (7 female, ages 15-16 years). Written consent from all the subjects were obtained from the subjects before the measurements. This study has been approved by the Ethical Review Board of Bogazici University.

5.4 Results

In order to observe MA induced variations in the neural complexity and concomitant functional clustering in the brain while seeking to correlate these variations with the heart rate and to be able to compare the results with those of [104], the subjects were divided into two groups: Subjects who show a big change in HR during task periods (high-HR) and subjects who show a moderate change during task periods (low-HR).

In terms of C_N, one can predict that complexity would increase during task periods with respect to rest periods; but the question that was sought to be answered was whether this increase would differ between high-HR and low-HR groups. Another aim was to explore the brain asymmetry during MA task using functional clustering. Based on published research results, we hypothesized that functional clusters would be more localized in the right prefrontal cortex for the high HR group. Whether the same pattern would be obtained for the low-HR group was the second major question to be answered.

NIRS parameters and HR indeed exhibit their expected patterns during the MA task, that is, oxy-Hb, total-Hb and HR all increase and deoxy-Hb decreases (see Figure 5.3. The changes during the second period pf MA task are generally smaller than the first task period for NIRS parameters for both of the groups whereas HR shows a different behavior for the two groups.

5.4.1 HR Changes

High-HR and low-HR groups were analyzed separately. Each group consisted of 7 subjects and Figure 5.4 shows the average HR for these groups for the task and control periods. Resting HR values are close to each other and HR returns to baseline values after the task periods. MA task causes an increase in both groups, but with the low-HR group it is much lower. High-HR group exhibits changes of 27.81 ± 8.21 and

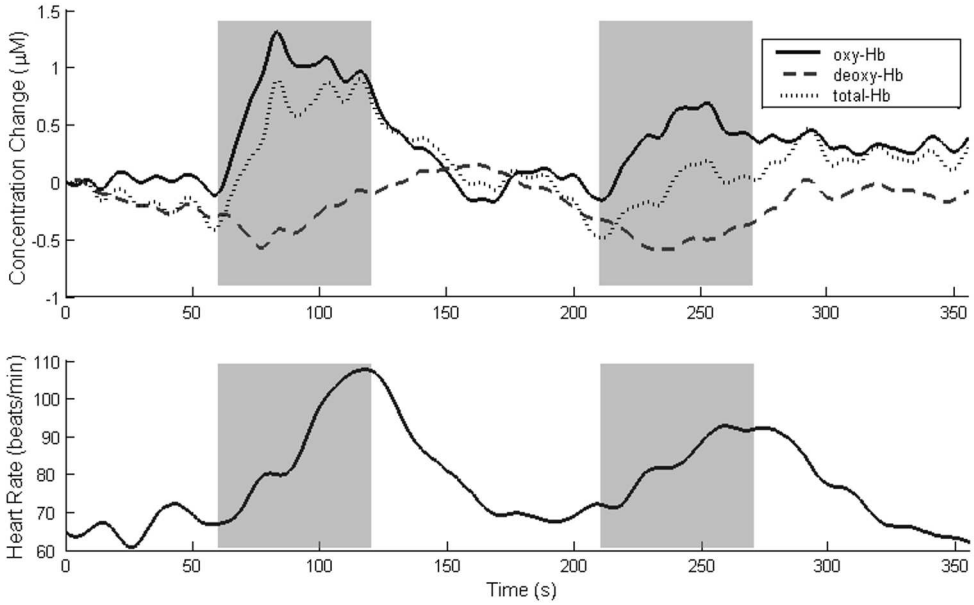

Figure 5.3 Typical examples of changes in NIRS parameters and heart rate during MA. Shaded areas denote the task period.

19.80 ± 12.58 for the first and second task periods, respectively. Low HR group exhibits changes of 8.91 ± 3.49 and 9.20 ± 8.49 for the first and second task periods, respectively. The difference between the amount of increases is statistically significant ($p < 0.001$) for the first task period, but insignificant for the second task period ($p = 0.089$). It may be noticed that the increase in HR is lower during the second task period for high-HR group whereas it is about the same for the low-HR group (although the differences between the task periods are not statistically significant for both of the groups). There may be two reasons for this phenomenon: First, since high-HR group exhibited a great increase, 90 seconds may not be enough for recovery, and therefore the second task period may take place on an elevated baseline. Although, the actual measurements show that the HR values return to their baseline values in the recovery period, this possibility cannot be totally eliminated. Second, subjects may get used to the experiment and experience less stress during the second task period. On the other hand, since low-HR group experience a smaller variation, that is the difference HR increases in the two succeeding periods is less pronounced, 90 seconds pause may be enough for recovery or the habituation effect (if any) is not observable.

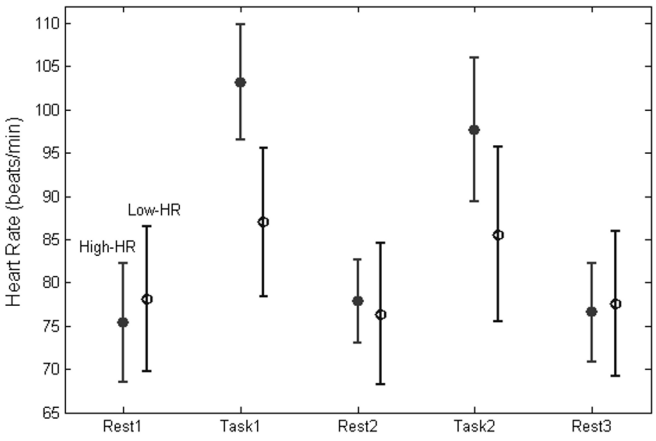

Figure 5.4 Heart rate changes for low and high-HR groups during each period of the experiment.

5.4.2 Changes in C_N

C_N values were calculated for every subject during each segment of the experiment. Figure 5.5 shows, for oxy-Hb, that although average values of the low-HR group are slightly lower than those of the high-HR group, they are not different significantly, in other words, they both increase. The results for deoxy-Hb and total-Hb (not shown) are also similar. The most striking observation is that C_N increases in the first task period for both of the groups, but then it gradually decreases. It does not increase for the second task period and it does not return to baseline values after the tasks during the recovery periods. Another observation is that low-HR group exhibited a lower value of C_N already at the first rest period.

5.4.3 Functional Clustering

In [104], it was shown that MA task induced activity was right lateral for high-HR subjects and left lateral for low-HR subjects. To evaluate the lateralization of the brain within the information-theoretic framework, the functional clusters were identified during the task periods. Figures 5.6 and 5.7 picture the functional clusters for oxy-Hb and deoxy-Hb, respectively. High-HR group showed a right-lateral clustering pattern for oxy-Hb during the first task period with small clusters in the medial parts;

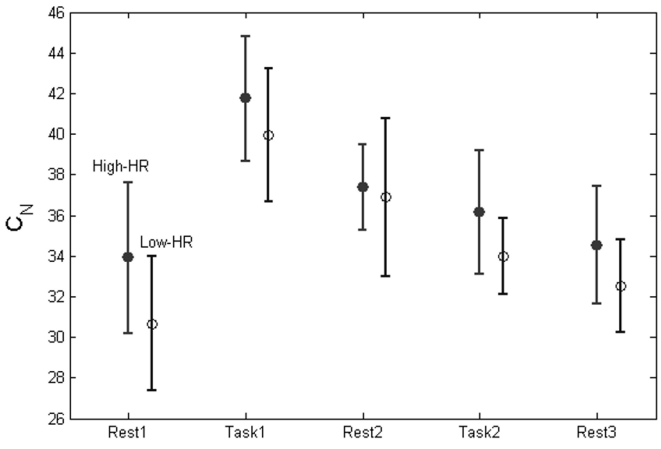

Figure 5.5 Change of neural complexity for oxy-Hb during each period of the experiment.

this right-lateralization continues during the second task period but in a more confined region and the clusters in the medial regions totally disappear. Low-HR group showed right medial clustering in the first task period and in the second task period new clusters emerge at the right lateral prefrontal cortex. Consequently, although functional clusters cover a smaller area during the second task period for the high-HR group, clusters become more wide-spread for low-HR group. However, all of the activity is always in the right hemisphere.

For deoxy-HB, clustering behavior of the brain during MA is different. High-HR group has right medial clusters both for the first and second task periods. The cluster becomes wider and stronger for the second task period. One important difference observed with the low-HR group was that this group showed a left lateral clustering in the first and second task periods in addition to right medial clusters. Interestingly, the right medial cluster is stronger in the first task period and becomes weaker in the second task period which is accompanied by the widening of the left lateral cluster.

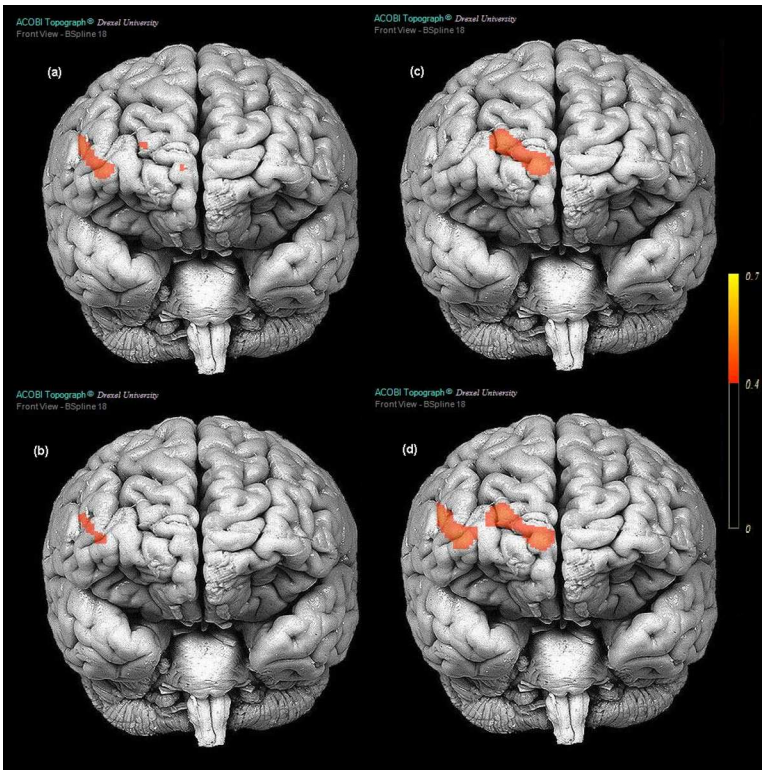

Figure 5.6 Functional clusters in the prefrontal cortex for oxy-Hb a) First task period high-HR group, b) Second task period high-HR group, c) First task period low-HR group, d) Second task period low-HR group.

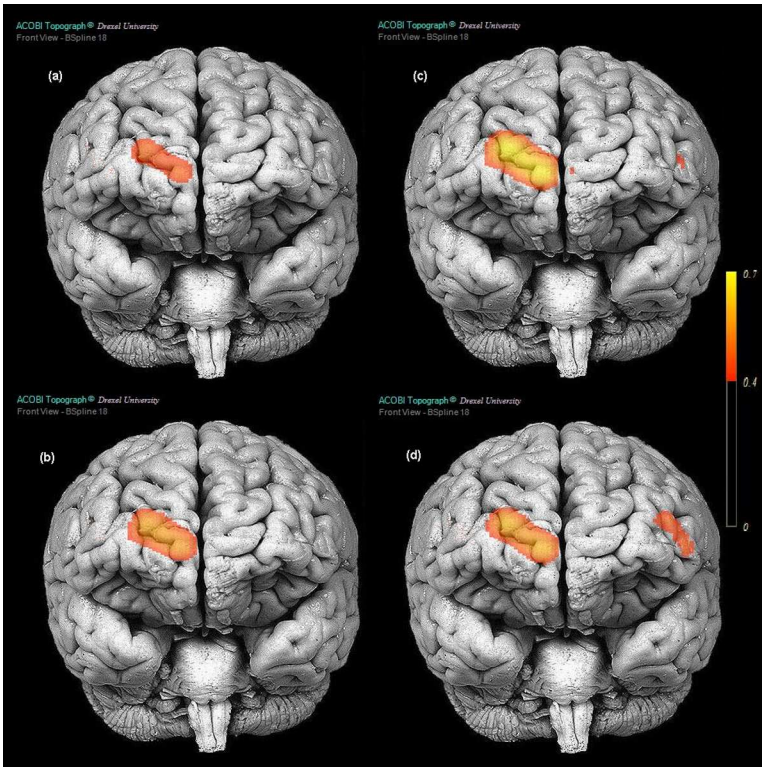

Figure 5.7 Functional clusters in the prefrontal cortex for deoxy-Hb a) First task period high-HR group, b) Second task period high-HR group, c) First task period low-HR group, d) Second task period low-HR group.

5.5 Discussion

The results confirm some of our predictions, while contradict some others. MA task caused a stress for all the subjects as evidenced by increases in HR during task periods. The NIRS parameters, in accordance with the HR values, albeit different, show changes for both of the task periods. However, C_N does not follow the same pattern. It increases for the first task period and then follows a continuously decreasing trend. This is an unexpected result since we were hypothesizing that neural complexity should always be higher during the task periods compared to rest conditions. This type of discrepancies was also reported by other researchers using the C_N [95, 97, 102]. In [97], an interesting result was also obtained such that the C_N of the recovery period at the end of the experiment was calculated to be higher than during the task period. These researchers put forward the possibility that subjects' brains might well be concentrated on some problems during rest which caused a higher complexity than the task. This point is also related with the much discussed "baseline" activity [109, 110]. C_N is related with the organization of the brain and is not dependent on the signal magnitudes. Hence, these results assert that although the magnitude of the signal increases for the second task period, organization of the brain does not become more complex as measured by the C_N metric.

Another point is that there were no significant differences between low-HR and high-HR groups during both rest and task periods. To compare this finding, we calculated for oxy-Hb and deoxy-Hb the average concentration change over all detectors during task periods. There was a significant difference ($p < 0.05$) between the groups for oxy-Hb during the first task period (0.71 ± 0.55 vs. 0.16 ± 0.37). The difference during the second task period was not significant. Deoxy-Hb concentration changes were not significantly different between the groups, either.

These findings on C_N may open a path to circumvent one of the major drawbacks of NIRS, that is, contribution of the extracerebral tissues when trying to observe the brain. HR changes are directly reflected on the circulation in the skin. Since the light of NIRS probes skin, scalp, cerebrospinal fluid and cerebral cortex, it is not

easy to extract the signal coming solely from the cortex. When the analysis is solely based on concentration changes, there is always the risk of identifying some "skin activation" as "cognitive activation." However, this risk may be lowered if concepts like neural complexity, which are not directly related to the magnitude of the signals but organizational aspects of this bundle of signals, are used.

Functional clustering analysis shows that there is a right dominance of the hemispheric activity during MA, for both of the high-HR and low-HR groups, but with the subtle difference that high-HR group shows a clear right lateralization whereas the low-HR group has strong clusters in the medial regions. The clusters become weaker in the second task period for high-HR group, while it becomes wider and stronger for the low-HR group. It may be conjectured that high-HR group exhibits an "exaggerated" response during the first task period which is lowered during the second task period with the effect of getting used to the experiment. However, the low-HR group does not show the same habituation effect. There is a consistent right medial clustering for deoxy-Hb for both of the groups for both of the task periods. It is interesting to note that there are also left lateral clusters for low-HR group. Previous research has shown that high-HR group has a right lateral activity whereas low-HR group has a left lateral activity [104]. Although our methods do not allow us to make a direct comparison with these findings, the left lateral clusters may have a similar origin. On the other hand, direct projections from the medial prefrontal cortex to brain stem and spinal regions which are associated with sympathetic vasomotor function have already been described [105]. These pathways have been implicated as mediating the cortically evoked circulatory responses.

In a review study [111], it was pointed out that a simple left/right dichotomy with respect to hemispheric specialization for the autonomic component of the emotional response was probably untenable noting that cortical and subcortical asymmetries in the central and autonomic nervous systems processing of emotional information might be reversed. Hence, hemispheric asymmetry should be treated with reservations and it should be avoided to make clear cut conclusions.

6. CONCLUSIONS

The previous three chapters tried to make a contribution to the debate on the capability of fNIRS for measuring cognitive activity. It would be appropriate to note that fNIRS has some inherent drawbacks which cannot be solely circumvented by signal processing techniques. However, effective algorithmic tools may be valuable in extracting the information carried by the signals and interpreting them. Owing to the literature on neuroimaging, this thesis study put forward statistical inference methods as the best candidate for this purpose and investigated their feasibility. It was found that MFX or Bayesian analysis of hierarchical GLMs may be used for identifying cognitive activity by fNIRS. This is the main conclusion of this study. This finding was then extended in two related routes. In the first route, constraining the GLM for sensible HRFs was investigated and it was shown that by using simple Bayesian techniques it became possible to make sure that the outcome of the analysis is a plausible HRF. This was important because identifying activations which are unrealistic clearly increases false positives of the analysis which is the greatest source of error in neuroimaging. The second route departed from hypothesis-based statistical inference and an introduction to the application of information-theoretic measures to fNIRS was made. Promising results were obtained showing that in the brain some organizational differences take place during cognitive activity which can be detected by these measures.

7. PERSPECTIVES

In the Introduction, it was stated that statistics is an effective way to separate noise from signal as long as the assumptions hold. Hence, the assumptions of this study also constitute the research areas of future work.

First of all, the assumption of whiteness about the noise may be reconsidered and a study on the temporal and spatial characteristics of the noise may be carried out. The popular autoregressive models may be investigated as the begining step.

The application of GLM is univariate in this study. This means that spatial dependencies between the detectors are not taken into account. It is known that this also causes the multiple comparison problem. By also exploiting the fact that fNIRS generally has a small number of detectors, a multivariate analysis method may be developed. Consequently, the multiple comparison problem for fNIRS signals may also be studied.

A strong assumption of the thesis is linearity. The linearity assumption is under investigation both for fNIRS, [112, 113, 114, 115], and fMRI, [116, 117]. Consequently, a future study may be planned investigating the validity of linearity assumption and nonlinear aspects of fNIRS signal.

An HRF model which was offered mainly for fMRI is used in this study. The accurate estimation of the HRF as measured by fNIRS remains as a further study. An exploratory approach may be adopted for this purpose. Bayesian and blind source separation techniques may have an important role in this task.

Another assumption which simplifies the analysis is that the hemodynamic response is constant in time. However, there are studies which puts this assumption under discussion [118, 119]. Hence, a model with a temporally varying HRF may be

developed to capture this time-dependent characteristics of hemodynamic response.

These suggestions for future work clearly imply a more sophisticated model. It may be conjectured that Bayesian methodology may manifest its potential better with these types of models. Accordingly, it may be suggested to concentrate more on Bayesian methods and develop tools that will better capture the characteristics of fNIRS data.

The suggestions till now are related with statistical inference framework. The usage of information-theoretic measures for fNIRS signals in this study should be considered as preliminary. Therefore this introduction may be enriched with additional methods. The Renyi entropy which was proven to be useful for EEG signals, [120] and which was partly investigated in the fNIRS framework, [121], may provide an initial starting point.

This thesis study limited itself with the observation of basic cognitive tasks. This was mainly because a particular goal of the study was to validate that fNIRS had the capability to measure cognitive activity and it would be better to concentrate on the basic functions. However, future work should definitely reconsider this point and try to find the best tasks that fNIRS is suitable for observing. BCI and emotion processing may open interesting study areas in this sense, since these are the tasks that the subjects should feel the least disturbance.

Improvement of the capabilities of fNIRS may come with the collective effort of different disciplines. This thesis study stood on the side of signal processing and tried to develop some basic routines for fNIRS signal analysis. Definitely, a more sophisticated integration between hardware design, algorithm development and theoretical and experimental physics will bring greater achievements.

APPENDIX A. STATISTICAL INFERENCE TECHNIQUES

The simplest structure of a hierarchical GLM is a two-level model which is used for determining average group activation. In a two-level hierarchical GLM (see Figure A.1, the first level models within-subject effects:

$$Y_k = X_k b_k + Z_k h_k + e_k \tag{A.1}$$

where Y_k is the N-sample fNIRS data for subject k, X_k is the $N \times p$ design matrix for the parameters of interest, b_k is the p vector of unknown parameters, Z_k is the $N \times m$ design matrix for the nuisance parameters, h_k is the q vector of unknown nuisance parameters, and e_k is the N-long error vector. Parameters of interest consist of cognitive components and nuisance parameters consist of some covariates, metabolic oscillations etc. We are assuming that the nuisance parameters are subject-specific whereas cognitive parameter vectors of individual subjects are representative samples from some population. Thus we proceed with,

$$b_k = X_{gk} b_g + e_{gk} \tag{A.2}$$

where X_{gk} is the $p \times q$ design matrix linking the subject's parameters to the group parameters, b_g is the q vector of group parameters, and e_{gk} is the p term error vector. In lieu of expression Eq. A.2, the group-level model can be written as,

$$b = X_g b_g + e_g \tag{A.3}$$

where b is the Kp dimensional concatenated parameter vector, X_g is the $Kp \times q$ group-level design matrix: $X_g = \begin{bmatrix} X_{g1} & X_{g2} & \cdots & X_{gK} \end{bmatrix}^T$, where, b_g is the q vector of group parameters and e_g is the Kp error vector. Note that, we carried all the parameters from the subject level to the group level, i.e. no contrasts were applied at the subject level. Thus, group-level model is inherently multivariate since it brings together the subject-level estimates (a vector) to arrive at a group decision. Define the matrix B such that its k^{th} row is constituted of the k^{th} subject's parameters: $B = \begin{bmatrix} b_1^T & b_2^T & \cdots & b_K^T \end{bmatrix}^T$.

If we introduce the $vec(.)$ operator, which stacks the columns of its matrix argument from left to right into a single vector, one can simply write $b = vec(B^T)$. Then,

$$B = X_g^m B_g + E_g \tag{A.4}$$

where X_g^m is the $K \times r$ group-level design matrix, B_g is the $r \times p$ matrix of group parameters, and E_g is the $K \times p$ error vector. Note that, $b_g = vec(B_g)$, $e_g = vec(E_g)$, and $r \times p = q$. Generally the group-level design matrices are simple. For example for average group activation, $X_g = 1_K \otimes I_p$, and $X_g^m = 1_K$, where 1_K stands for a K vector of *1*'s and $\otimes$ is the Kronecker product. In this case, $p = q$ and $r = 1$. The probability distribution function (pdf) of the subject-level error vector is assumed to be Gaussian with no temporal correlation, that is, $cov(e_k) = \sigma_k^2 \times I_N$. Since the group-level model is multivariate, the definition of the covariance for the error matrix should take into account the two sources of variability: within and between subjects. Consider the following definition of covariance for the error vector in Eq. A.3:

$$cov(e_g) = \Phi \otimes \Sigma$$

where Φ is the between-subjects covariance matrix, and Σ is the within-subject covariance matrix. Recall that we are now dealing with parameter estimates of the subjects. Hence, "within" and "between" refer to the parameters, unlike the first level in which "within" refers to the subjects' time series. Since we are assuming that the subjects are drawn independently and identically from a population, Φ is a $K \times K$ identity matrix, that is, $\Phi = I_K$, whereas the $p \times p$ within-subject covariance matrix Σ is some positive definite matrix. We have no prior information about Σ and hence we will assume that it has a general structure. Define $\Sigma = C_g$, where C_g is positive definite. Consequently,

$$cov(e_g) = I_K \otimes C_g = C_G \tag{A.5}$$

Having defined the variables we may proceed with the steps specific to classical and Bayesian inference.

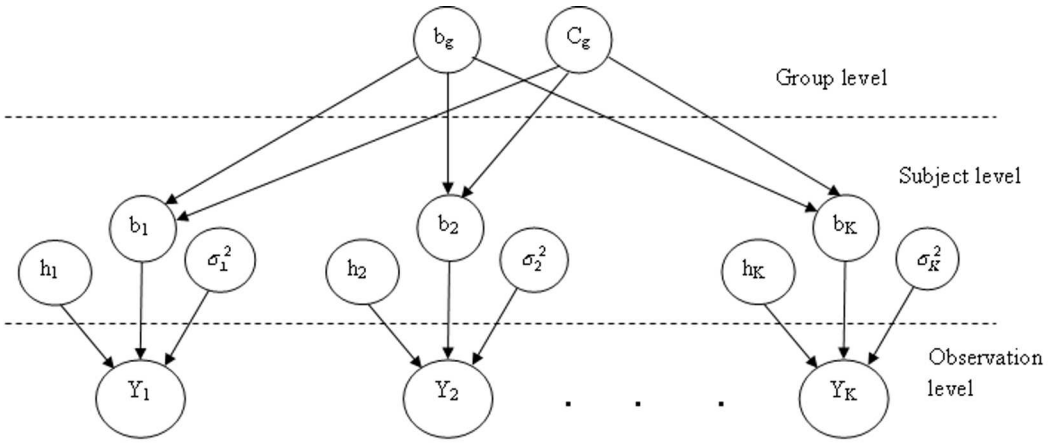

Figure A.1 Two-level GLM for average group activation.

A.1 Classical Inference

For the ease of expositions, begin by concatenating the design matrices and parameter vectors and define, $X_k^c = \left[\begin{array}{ccc} X_k & \vdots & Z_k \end{array} \right]$, and $b_k^c = \left[\begin{array}{ccc} b_k^T & \vdots & h_k^T \end{array} \right]^T$ Ordinary least squares estimate of b_k^c is given by,

$$\hat{b}_k^c = \left(X_k^{cT} X_k^c \right)^{-1} X_k^{cT} Y_k \tag{A.6}$$

This estimate has variance,

$$cov(\hat{b}_k^c) = \sigma_k^2 \left(X_k^{cT} X_k^c \right)^{-1}, \tag{A.7}$$

where the noise variance, σ_k^2, is estimated from the residuals. In the summary-statistics approach to multilevel GLM, the second level of the model takes as input the estimates of the first level but not the true (and unobservable) parameters [122]. Hence, the second level (Eq. A.3) model is modified as:

$$\hat{b} = X_g b_g + e_g + \left(\hat{b} - b \right) = X_g b_g + \hat{e}_g. \tag{A.8}$$

Then, the variance of the error vector, $\hat{e}_g$, is,

$$V_{\hat{g}} = diag\left(\left(\sigma_k^2 (X_k^{cT} X_k^c)^{-1} \right) \right) + \sigma_g^2 C_g, \tag{A.9}$$

The first component of the variance specifies the within subject variance-covariance of the parameter vector (fixed effects) and the second component indicates the between subjects variance (random effects). Since, generally the desired inference is on a particular contrast of parameters, cb_k, $\hat{b}$ becomes $\hat{b}_{cont} = \left[\begin{array}{ccc} c\hat{b}_1 & \ldots & c\hat{b}_K \end{array} \right]^T$ .. Subject-level error variances become then,

$$cov\left(c\hat{b}_k\right) = \sigma_k^2 c \left(X_k^{cT} X_k^c\right)^{-1} c^T \tag{A.10}$$

and C_g has a simple form, typically I_K. Summary-statistics MFX procedure accounts for both of these sources of variance whereas FFX and RFX ignore the second and first components of the variance, respectively.

A.2 Bayesian Inference

To derive the equations for Bayesian inference we will begin from Eq. A.1, Eq. A.2, Eq. A.3 and Figure A.1. The conditional posterior pdf's can be written using the Bayesian rule (posterior α prior $\times$ likelihood):

$$p\left(b_k|M, r.v.\right) \ \alpha \ p\left(b_k|M, b_g, C_g\right) \ p\left(Y_k|M, b_k, h_k, \sigma_k^2\right), \tag{A.11}$$

$$p\left(h_k|M, r.v.\right) \ \alpha \ p\left(h_k|M\right) \ p\left(Y_k|M, b_k, h_k, \sigma_k^2\right), \tag{A.12}$$

$$p\left(\sigma_k^2|M, r.v.\right) \ \alpha \ p\left(\sigma_k^2|M\right) \ p\left(Y_k|M, b_k, h_k, \sigma_k^2\right), \tag{A.13}$$

$$p\left(b_g|M, r.v.\right) \ \alpha \ p\left(b_g|M\right) \prod_{k=1:K} p\left(b_k|M, b_g, C_g\right), \tag{A.14}$$

$$p\left(C_g|M, r.v.\right) \ \alpha \ p\left(C_g|M\right) \prod_{k=1:K} p\left(b_k|M, b_g, C_g\right). \tag{A.15}$$

where $r.v$ stands for remaining variables. We need to specify prior distributions for h_k, σ_k^2, b_g, and C_g to be able to derive conditional posterior pdf's. Since prior information

about the distributions of these variables is typically not available, we decided to use noninformative priors. Note that we do not have to specify priors for subject-level parameter estimates, b_k, since the group parameters in the model hierarchy act as the priors of subjects' parameters.

The conditional posterior of subject level parameters depend on both subjects' data and group level parameters. If we write Eq. A.11 explicitly,

$$p\left(b_k|M,r.v.\right)\ \alpha\ \left|C_g\right|^{-1/2}\ exp\left\{-\left(b_k-X_{gk}b_g\right)^T C_g^{-1}\left(b_k-X_{gk}b_g\right)\right\} \qquad (A.16)$$
$$\times\sigma_k^{-N/2}\ exp\left\{-\left(Y_k-X_kb_k-Z_kh_k\right)^T\left(Y_k-X_kb_k-Z_kh_k\right)/\sigma_k^2\right\}.$$

The conditional posterior of subject level parameters are the product of two Gaussian distributions, hence they are also Gaussian. Actually, subjects' parameters are estimated from data and instantaneous group parameter estimates inversely weighted with their corresponding variance estimates.

The noninformative prior for nuisance parameters are the uniform distribution, and consequently their conditional posterior is just the likelihood term:

$$p\left(h_k|M,r.v.\right)\ \alpha\ \sigma_k^{-N/2}\ exp\left\{-\left(Y_k-X_kb_k-Z_kh_k\right)^T\left(Y_k-X_kb_k-Z_kh_k\right)/\sigma_k^2\right\}. \quad (A.17)$$

The noninformative Jeffreys prior for subject level error variance is, $p\left(\sigma_k^2|M\right)\alpha\ \sigma_k^{-2}$. Consequently, we can write Eq. A.13 as,

$$p\left(\sigma_k^2|M,r.v.\right)\ \alpha\ \sigma_k^{-(N+2)/2}\ exp\left\{-\left(Y_k-X_kb_k-Z_kh_k\right)^T\left(Y_k-X_kb_k-Z_kh_k\right)/\sigma_k^2\right\}. \qquad (A.18)$$

Hence, conditional posteriors for subject level variances are inverse Gamma.

Since the noninformative prior for group level parameters is the uniform distribution, the conditional posterior of them may be written as,

$$p\left(b_g|M,r.v.\right)\ \alpha\ \left|C_G\right|^{-1/2}\ exp\left\{-\left(b-X_gb_g\right)^T C_G^{-1}\left(b-X_gb_g\right)\right\}, \qquad (A.19)$$

which is a multivariate Gaussian distribution.

C_g models the dependencies among the elements of the subject level parameter estimates. The noninformative prior for group level error variance is, $p\left(C_g|M\right)\ \alpha\ |C_g|^{-1}$. The conditional posterior may be written as,

$$p\left(C_g|M\right)\ \alpha\ |C_g|^{-(K+2)/2}\ exp\left\{trC_g^{-1}\left(B-X_g^mB_g\right)^T\left(B-X_g^mB_g\right)\right\}. \tag{A.20}$$

Finally, group covariance matrix has conditionally an inverse-Wishart distribution [51].

The consequence of assuming Gaussian distributions for noise vectors and using noninformative priors is that conditional posterior pdf's have analytical forms whose modes can be easily calculated. Thus, we may proceed with an algorithm like iterated conditional modes (ICM) [50]. Beginning from some initial values we may cycle through the modes until convergence. The algorithm is summarized below:

$$\hat{b}_k=\left(C_g^{-1}+\sigma_k^{-2}X_k^TX_k\right)^{-1}\left(C_g^{-1}+\sigma_k^{-2}X_k^T\left(Y_k-Z_kh_k\right)\right), \tag{A.21}$$

$$\hat{h}_k=\left(Z_k^TZ_k\right)^{-1}Z_k^T\left(Y_k-X_kb_k\right), \tag{A.22}$$

$$\hat{\sigma}_k^2=\frac{\left(Y_k-X_kb_k-Z_kh_k\right)^T\left(Y_k-X_kb_k-Z_kh_k\right)}{N+2}, \tag{A.23}$$

$$\hat{b}_g=\left(X_g^TC_G^{-1}X_g\right)^{-1}X_g^TC_G^{-1}b, \tag{A.24}$$

$$\hat{C}_g=\frac{\left(B-X_g^mB_g\right)^T\left(B-X_g^mB_g\right)}{K+2}. \tag{A.25}$$

REFERENCES

1. Jöbsis, F., "Noninvasive, infrared monitoring of cerebral and myocardial oxygen sufficiency and circulatory parameters," *Science*, Vol. 198, pp. 1264–1267, Dec 1977.

2. Herrmann, M. J., M. M. Plichta, A.-C. Ehlis, and A. J. Fallgatter, "Optical topography during a go-nogo task assessed with multi-channel near-infrared spectroscopy," *Behav Brain Res*, Vol. 160, pp. 135–140, May 2005.

3. Fallgatter, A. J., and W. K. Strik, "Right frontal activation during the continuous performance test assessed with near-infrared spectroscopy in healthy subjects," *Neurosci Lett*, Vol. 223, pp. 89–92, Feb 1997.

4. Kubota, Y., M. Toichi, M. Shimizu, R. A. Mason, R. L. Findling, K. Yamamoto, and J. R. Calabrese, "Prefrontal hemodynamic activity predicts false memory–a near-infrared spectroscopy study," *Neuroimage*, Vol. 31, pp. 1783–1789, Jul 2006.

5. Hatakenaka, M., I. Miyai, M. Mihara, S. Sakoda, and K. Kubota, "Frontal regions involved in learning of motor skill–a functional nirs study," *Neuroimage*, Vol. 34, pp. 109–116, Jan 2007.

6. Hirth, C., H. Obrig, K. Villringer, A. Thiel, J. Bernarding, W. Mühlnickel, H. Flor, U. Dirnagl, and A. Villringer, "Non-invasive functional mapping of the human motor cortex using near-infrared spectroscopy," *Neuroreport*, Vol. 7, pp. 1977–1981, Aug 1996.

7. Franceschini, M. A., S. Fantini, J. H. Thompson, J. P. Culver, and D. A. Boas, "Hemodynamic evoked response of the sensorimotor cortex measured noninvasively with near-infrared optical imaging," *Psychophysiology*, Vol. 40, pp. 548–560, Jul 2003.

8. Miyai, I., H. C. Tanabe, I. Sase, H. Eda, I. Oda, I. Konishi, Y. Tsunazawa, T. Suzuki, T. Yanagida, and K. Kubota, "Cortical mapping of gait in humans: a near-infrared spectroscopic topography study," *Neuroimage*, Vol. 14, pp. 1186–1192, Nov 2001.

9. Watanabe, E., Y. Yamashita, A. Maki, Y. Ito, and H. Koizumi, "Non-invasive functional mapping with multi-channel near infra-red spectroscopic topography in humans," *Neurosci Lett*, Vol. 205, pp. 41–44, Feb 1996.

10. Kato, T., A. Kamei, S. Takashima, and T. Ozaki, "Human visual cortical function during photic stimulation monitoring by means of near-infrared spectroscopy," *J Cereb Blood Flow Metab*, Vol. 13, pp. 516–520, May 1993.

11. Igawa, M., Y. Atsumi, K. Takahashi, S. Shiotsuka, H. Hirasawa, R. Yamamoto, A. Maki, Y. Yamashita, and H. Koizumi, "Activation of visual cortex in rem sleep measured by 24-channel nirs imaging," *Psychiatry Clin Neurosci*, Vol. 55, pp. 187–188, Jun 2001.

12. Uludağ, K., J. Steinbrink, M. Kohl-Bareis, R. Wenzel, A. Villringer, and H. Obrig, "Cytochrome-c-oxidase redox changes during visual stimulation measured by near-infrared spectroscopy cannot be explained by a mere cross talk artefact," *Neuroimage*, Vol. 22, pp. 109–119, May 2004.

13. Karen, T., G. Morren, D. Haensse, A. S. Bauschatz, H. U. Bucher, and M. Wolf, "Hemodynamic response to visual stimulation in newborn infants using functional near-infrared spectroscopy," *Hum Brain Mapp*, Vol. 29, pp. 453–460, Apr 2008.

14. Weber, P., J. Lütschg, and H. Fahnenstich, "Methylphenidate-induced changes in cerebral hemodynamics measured by functional near-infrared spectroscopy," *J Child Neurol*, Vol. 22, pp. 812–817, Jul 2007.

15. Ehlis, A.-C., C. G. Bähne, C. P. Jacob, M. J. Herrmann, and A. J. Fallgatter, "Reduced lateral prefrontal activation in adult patients with attention-deficit/hyperactivity disorder (adhd) during a working memory task: A functional near-infrared spectroscopy (fnirs) study," *J Psychiatr Res*, Jan 2008.

16. Suto, T., M. Fukuda, M. Ito, T. Uehara, and M. Mikuni, "Multichannel near-infrared spectroscopy in depression and schizophrenia: cognitive brain activation study," *Biol Psychiatry*, Vol. 55, pp. 501–511, Mar 2004.

17. Shinba, T., M. Nagano, N. Kariya, K. Ogawa, T. Shinozaki, S. Shimosato, and Y. Hoshi, "Near-infrared spectroscopy analysis of frontal lobe dysfunction in schizophrenia," *Biol Psychiatry*, Vol. 55, pp. 154–164, Jan 2004.

18. Herrmann, M. J., A.-C. Ehlis, and A. J. Fallgatter, "Prefrontal activation through task requirements of emotional induction measured with nirs," *Biol Psychol*, Vol. 64, pp. 255–263, Nov 2003.

19. Leon-Carrion, J., J. Damas, K. Izzetoglu, K. Pourrezai, J. F. Martín-Rodríguez, J. M. B. y Martin, and M. R. Dominguez-Morales, "Differential time course and intensity of pfc activation for men and women in response to emotional stimuli: a functional near-infrared spectroscopy (fnirs) study," *Neurosci Lett*, Vol. 403, pp. 90–95, Jul 2006.

20. Yang, H., Z. Zhou, Y. Liu, Z. Ruan, H. Gong, Q. Luo, and Z. Lu, "Gender difference in hemodynamic responses of prefrontal area to emotional stress by near-infrared spectroscopy," *Behav Brain Res*, Vol. 178, pp. 172–176, Mar 2007.

21. Coyle, S., T. Ward, C. Markham, and G. McDarby, "On the suitability of near-infrared (nir) systems for next-generation brain-computer interfaces," *Physiol Meas*, Vol. 25, pp. 815–822, Aug 2004.

22. Birbaumer, N., C. Weber, C. Neuper, E. Buch, K. Haapen, and L. Cohen, "Physiological regulation of thinking: brain-computer interface (bci) research," *Prog Brain Res*, Vol. 159, pp. 369–391, 2006.

23. Sitaram, R., H. Zhang, C. Guan, M. Thulasidas, Y. Hoshi, A. Ishikawa, K. Shimizu, and N. Birbaumer, "Temporal classification of multichannel near-infrared spectroscopy signals of motor imagery for developing a brain-computer interface," *Neuroimage*, Vol. 34, pp. 1416–1427, Feb 2007.

24. Bauernfeind, G., R. Leeb, S. C. Wriessnegger, and G. Pfurtscheller, "Development, set-up and first results for a one-channel near-infrared spectroscopy system," *Biomed Tech (Berl)*, Vol. 53, no. 1, pp. 36–43, 2008.

25. Hoshi, Y., and S. Chen, "Regional cerebral blood flow changes associated with emotions in children," *Pediatr Neurol*, Vol. 27, pp. 275–281, Oct 2002.

26. Bunce, S. C., M. Izzetoglu, K. Izzetoglu, B. Onaral, and K. Pourrezaei, "Functional near-infrared spectroscopy," *IEEE Eng Med Biol Mag*, Vol. 25, no. 4, pp. 54–62, 2006.

27. Schroeter, M. L., M. M. Bücheler, K. Müller, K. Uludağ, H. Obrig, G. Lohmann, M. Tittgemeyer, A. Villringer, and D. Y. von Cramon, "Towards a standard analysis for functional near-infrared imaging," *Neuroimage*, Vol. 21, pp. 283–290, Jan 2004.

28. Petersson, K. M., T. E. Nichols, J. B. Poline, and A. P. Holmes, "Statistical limitations in functional neuroimaging. i. non-inferential methods and statistical models," *Philos Trans R Soc Lond B Biol Sci*, Vol. 354, pp. 1239–1260, Jul 1999.

29. Friston, K., A. Holmes, J. B. Poline, C. Frith, and R. Frackowiak, "Statistical parametric maps in functional imaging: A general linear approach," *Human Brain Mapping*, Vol. 2, pp. 189–210, 1995.

30. Cope, M., and D. T. Delpy, "System for long-term measurement of cerebral blood and tissue oxygenation on newborn infants by near infra-red transillumination," *Med Biol Eng Comput*, Vol. 26, pp. 289–294, May 1988.

31. Delpy, D. T., M. Cope, P. van der Zee, S. Arridge, S. Wray, and J. Wyatt, "Estimation of optical pathlength through tissue from direct time of flight measurement," *Phys Med Biol*, Vol. 33, pp. 1433–1442, Dec 1988.

32. Duncan, A., J. H. Meek, M. Clemence, C. E. Elwell, L. Tyszczuk, M. Cope, and D. T. Delpy, "Optical pathlength measurements on adult head, calf and forearm and the head of the newborn infant using phase resolved optical spectroscopy," *Phys Med Biol*, Vol. 40, pp. 295–304, Feb 1995.

33. Roy, C. S., and C. S. Sherrington, "On the regulation of the blood-supply of the brain," *J Physiol*, Vol. 11, pp. 85–158.17, Jan 1890.

34. Emir, U., "System characterization for a fast optical imager," Master's thesis, Institute of Biomedical Engineering, Boğaziçi University, 2003.

35. Akin, A., D. Bilensoy, U. E. Emir, M. Gülsoy, S. Candansayar, and H. Bolay, "Cerebrovascular dynamics in patients with migraine: near-infrared spectroscopy study," *Neurosci Lett*, Vol. 400, pp. 86–91, May 2006.

36. Akgül, C. B., B. Sankur, and A. Akin, "Spectral analysis of event-related hemodynamic responses in functional near infrared spectroscopy," *J Comput Neurosci*, Vol. 18, no. 1, pp. 67–83, 2005.

37. Akgül, C. B., A. Akin, and B. Sankur, "Extraction of cognitive activity-related waveforms from functional near-infrared spectroscopy signals," *Med Biol Eng Comput*, Vol. 44, pp. 945–958, Nov 2006.

38. Boas, D. A., K. Chen, D. Grebert, and M. A. Franceschini, "Improving the diffuse optical imaging spatial resolution of the cerebral hemodynamic response to brain activation in humans," *Opt Lett*, Vol. 29, pp. 1506–1508, Jul 2004.

39. Fabbri, F., A. Sassaroli, M. E. Henry, and S. Fantini, "Optical measurements of absorption changes in two-layered diffusive media," *Phys Med Biol*, Vol. 49, pp. 1183–1201, Apr 2004.

40. Firbank, M., E. Okada, and D. T. Delpy, "A theoretical study of the signal contribution of regions of the adult head to near-infrared spectroscopy studies of visual evoked responses," *Neuroimage*, Vol. 8, pp. 69–78, Jul 1998.

41. Friston, K. J., W. Penny, C. Phillips, S. Kiebel, G. Hinton, and J. Ashburner, "Classical and bayesian inference in neuroimaging: theory," *Neuroimage*, Vol. 16, pp. 465–483, Jun 2002.

42. Friston, K. J., D. E. Glaser, R. N. A. Henson, S. Kiebel, C. Phillips, and J. Ashburner, "Classical and bayesian inference in neuroimaging: applications," *Neuroimage*, Vol. 16, pp. 484–512, Jun 2002.

43. Plichta, M. M., S. Heinzel, A.-C. Ehlis, P. Pauli, and A. J. Fallgatter, "Model-based analysis of rapid event-related functional near-infrared spectroscopy (nirs) data: a parametric validation study," *Neuroimage*, Vol. 35, pp. 625–634, Apr 2007.

44. Cohen-Adad, J., S. Chapuisat, J. Doyon, S. Rossignol, J.-M. Lina, H. Benali, and F. Lesage, "Activation detection in diffuse optical imaging by means of the general linear model," *Med Image Anal*, Vol. 11, pp. 616–629, Dec 2007.

45. Ciftci, K., B. Sankur, Y. P. Kahya, and A. Akın, "Multilevel statistical inference from functional near infrared spectroscopy data during stroop interference," *IEEE Transactions on Biomedical Engineering*, 2008. doi: 10.1109/TBME.2008.923918.

46. Neumann, J., and G. Lohmann, "Bayesian second-level analysis of functional magnetic resonance images," *Neuroimage*, Vol. 20, pp. 1346–1355, Oct 2003.

47. Beckmann, C. F., M. Jenkinson, and S. M. Smith, "General multilevel linear modeling for group analysis in fmri," *Neuroimage*, Vol. 20, pp. 1052–1063, Oct 2003.

48. Woolrich, M. W., T. E. J. Behrens, C. F. Beckmann, M. Jenkinson, and S. M. Smith, "Multilevel linear modelling for fmri group analysis using bayesian inference," *Neuroimage*, Vol. 21, pp. 1732–1747, Apr 2004.

49. Thirion, B., P. Pinel, S. Meriaux, A. Roche, S. Dehaene, and J. Poline, "Analysis of a large fmri cohort: Statistical and methodological issues for group analyses," *Neuroimage*, Vol. 35, pp. 105–120, 2007.

50. Rowe, D. B., *Multivariate Bayesian Statistics: Models for Source Separation and Signal Unmixing*, Chapman & Hall/CRC, 2003.

51. Gelman, A. B., J. S. Carlin, H. S. Stern, and D. B. Rubin, *Bayesian Data Analysis*, Chapman & Hall/CRC, 1995.

52. MacLeod, C. M., "Half a century of research on the stroop effect: an integrative review," *Psychol Bull*, Vol. 109, pp. 163–203, Mar 1991.

53. Büyükaksoy, G. K., N. S. Şengör, H. Gürvit, and C. Güzeliş, "Modelling the stroop effect: A connectionist approach," *Neurocomputing*, Vol. 70, pp. 1414–1423, 2007.

54. Zysset, S., K. Müller, G. Lohmann, and D. Y. von Cramon, "Color-word matching stroop task: separating interference and response conflict," *Neuroimage*, Vol. 13, pp. 29–36, Jan 2001.

55. Friston, K. J., P. Fletcher, O. Josephs, A. Holmes, M. D. Rugg, and R. Turner, "Event-related fmri: characterizing differential responses," *Neuroimage*, Vol. 7, pp. 30–40, Jan 1998.

56. Friston, K. J., O. Josephs, E. Zarahn, A. P. Holmes, S. Rouquette, and J. Poline, "To smooth or not to smooth? bias and efficiency in fmri time-series analysis," *Neuroimage*, Vol. 12, pp. 196–208, Aug 2000.

57. Mitchell, R. L. C., "The bold response during stroop task-like inhibition paradigms: Effects of task difficulty and task-relevant modality," *Brain Cogn*, Vol. 59, pp. 23–37, Oct 2005.

58. Bench, C. J., C. D. Frith, P. M. Grasby, K. J. Friston, E. Paulesu, R. S. Frackowiak, and R. J. Dolan, "Investigations of the functional anatomy of attention using the stroop test," *Neuropsychologia*, Vol. 31, pp. 907–922, Sep 1993.

59. Villringer, A., and B. Chance, "Non-invasive optical spectroscopy and imaging of human brain function," *Trends Neurosci*, Vol. 20, pp. 435–442, Oct 1997.

60. Schroeter, M. L., S. Cutini, M. M. Wahl, R. Scheid, and D. Y. von Cramon, "Neurovascular coupling is impaired in cerebral microangiopathy–an event-related stroop study," *Neuroimage*, Vol. 34, pp. 26–34, Jan 2007.

61. Heller, R., Y. Golland, R. Malach, and Y. Benjamini, "Conjunction group analysis: an alternative to mixed/random effect analysis," *Neuroimage*, Vol. 37, pp. 1178–1185, Oct 2007.

62. Chow, S. L., *Statistical Significance: Rationale, Validity and Utility*, SAGE Publications, 1996.

63. Woolrich, M. W., T. E. J. Behrens, and S. M. Smith, "Constrained linear basis sets for hrf modelling using variational bayes," *Neuroimage*, Vol. 21, pp. 1748–1761, Apr 2004.

64. Logan, B. R., and D. B. Rowe, "An evaluation of thresholding techniques in fmri analysis," *Neuroimage*, Vol. 22, pp. 95–108, May 2004.

65. Singh, A. K., and I. Dan, "Exploring the false discovery rate in multichannel nirs," *Neuroimage*, Vol. 33, pp. 542–549, Nov 2006.

66. Schroeter, M. L., S. Zysset, T. Kupka, F. Kruggel, and D. Y. von Cramon, "Near-infrared spectroscopy can detect brain activity during a color-word matching stroop task in an event-related design," *Hum Brain Mapp*, Vol. 17, pp. 61–71, Sep 2002.

67. Ehlis, A.-C., M. J. Herrmann, A. Wagener, and A. J. Fallgatter, "Multi-channel near-infrared spectroscopy detects specific inferior-frontal activation during incongruent stroop trials," *Biol Psychol*, Vol. 69, pp. 315–331, Jul 2005.

68. Hoshi, Y., N. Kobayashi, and M. Tamura, "Interpretation of near-infrared spectroscopy signals: a study with a newly developed perfused rat brain model," *J Appl Physiol*, Vol. 90, pp. 1657–1662, May 2001.

69. Plichta, M. M., M. J. Herrmann, C. G. Baehne, A.-C. Ehlis, M. M. Richter, P. Pauli, and A. J. Fallgatter, "Event-related functional near-infrared spectroscopy (fnirs): are the measurements reliable?," *Neuroimage*, Vol. 31, pp. 116–124, May 2006.

70. Buxton, R. B., E. C. Wong, and L. R. Frank, "Dynamics of blood flow and oxygenation changes during brain activation: the balloon model," *Magn Reson Med*, Vol. 39, pp. 855–864, Jun 1998.

71. Strangman, G., J. P. Culver, J. H. Thompson, and D. A. Boas, "A quantitative comparison of simultaneous bold fmri and nirs recordings during functional brain activation," *Neuroimage*, Vol. 17, pp. 719–731, Oct 2002.

72. Huppert, T. J., R. D. Hoge, S. G. Diamond, M. A. Franceschini, and D. A. Boas, "A temporal comparison of bold, asl, and nirs hemodynamic responses to motor stimuli in adult humans," *Neuroimage*, Vol. 29, pp. 368–382, Jan 2006.

73. Friman, O., M. Borga, P. Lundberg, and H. Knutsson, "Adaptive analysis of fmri data," *Neuroimage*, Vol. 19, pp. 837–845, Jul 2003.

74. Ciftci, K., B. Sankur, Y. P. Kahya, and A. Akın, "Constraining the general linear model for sensible hemodynamic response function waveforms," *Med Biol Eng Comput*, Apr 2008. doi 10.1007/s11517-008-0347-6.

75. Steinbrink, J., A. Villringer, F. Kempf, D. Haux, S. Boden, and H. Obrig, "Illuminating the bold signal: combined fmri-fnirs studies," *Magn Reson Imaging*, Vol. 24, pp. 495–505, May 2006.

76. Buxton, R. B., K. Uludağ, D. J. Dubowitz, and T. T. Liu, "Modeling the hemodynamic response to brain activation," *Neuroimage*, Vol. 23 Suppl 1, pp. S220–S233, 2004.

77. de Zwart, J. A., A. C. Silva, P. van Gelderen, P. Kellman, M. Fukunaga, R. Chu, A. P. Koretsky, J. A. Frank, and J. H. Duyn, "Temporal dynamics of the bold fmri impulse response," *Neuroimage*, Vol. 24, pp. 667–677, Feb 2005.

78. Handwerker, D. A., J. M. Ollinger, and M. D'Esposito, "Variation of bold hemodynamic responses across subjects and brain regions and their effects on statistical analyses," *Neuroimage*, Vol. 21, pp. 1639–1651, Apr 2004.

79. Schroeter, M. L., S. Zysset, M. Wahl, and D. Y. von Cramon, "Prefrontal activation due to stroop interference increases during development–an event-related fnirs study," *Neuroimage*, Vol. 23, pp. 1317–1325, Dec 2004.

80. Suzuki, M., I. Miyai, T. Ono, and K. Kubota, "Activities in the frontal cortex and gait performance are modulated by preparation. an fnirs study," *Neuroimage*, Vol. 39, pp. 600–607, Jan 2008.

81. Devroye, L., *Non-uniform random variate generation*, Springer., 1986.

82. Worsley, K. J., and J. E. Taylor, "Detecting fmri activation allowing for unknown latency of the hemodynamic response," *Neuroimage*, Vol. 29, pp. 649–654, Jan 2006.

83. Gelfand, A., A. Smith, and T. Lee, "Analysis of constrained parameter and truncated data problems using sampling," *Journal of the American Statistical Association*, Vol. 87, pp. 523–532, 1992.

84. Smith, A., and G. Roberts, "Bayesian computation via the gibbs sampler and related markov chain monte carlo methods," *Journal of the Royal Statistical Society, Series B (Methodological)*, Vol. 55, pp. 3–23, 1993.

85. Dunson, D. B., and B. Neelon, "Bayesian inference on order-constrained parameters in generalized linear models," *Biometrics*, Vol. 59, pp. 286–295, Jun 2003.

86. Smith, A. T., K. D. Singh, and J. H. Balsters, "A comment on the severity of the effects of non-white noise in fmri time-series," *Neuroimage*, Vol. 36, pp. 282–288, Jun 2007.

87. Purdon, P. L., and R. M. Weisskoff, "Effect of temporal autocorrelation due to physiological noise and stimulus paradigm on voxel-level false-positive rates in fmri," *Hum Brain Mapp*, Vol. 6, no. 4, pp. 239–249, 1998.

88. Woolrich, M. W., B. D. Ripley, M. Brady, and S. M. Smith, "Temporal autocorrelation in univariate linear modeling of fmri data," *Neuroimage*, Vol. 14, pp. 1370–1386, Dec 2001.

89. Tononi, G., O. Sporns, and G. M. Edelman, "A measure for brain complexity: relating functional segregation and integration in the nervous system," *Proc Natl Acad Sci U S A*, Vol. 91, pp. 5033–5037, May 1994.

90. Crutchfield, J., and N. Packard, "Symbolic dynamics of noisy chaos," *Physica D: Nonlinear Phenomena*, Vol. Volume 7, pp. 201–223., 1983.

91. Crutchfield, and Young, "Inferring statistical complexity," *Phys Rev Lett*, Vol. 63, pp. 105–108, Jul 1989.

92. Feldman, D. P., and J. P. Crutchfield, "Structural information in two-dimensional patterns: entropy convergence and excess entropy," *Phys Rev E Stat Nonlin Soft Matter Phys*, Vol. 67, p. 051104, May 2003.

93. Young, K., and N. Schuff, "Measuring structural complexity in brain images," *Neuroimage*, Vol. 39, pp. 1721–1730, Feb 2008.

94. Friston, K., G. Tononi, O. Sporns, and G. Edelman, "Characterising the complexity of neuronal interactions," *Human Brain Mapping*, Vol. 3, pp. 302–314, 1995.

95. van Putten, K., and C. Stam, "Application of a neural complexity measure to multichannel eeg," *Phys. Lett. A*, Vol. 281, pp. 131–141, 2001.

96. Branston, N. M., W. El-Deredy, and F. P. McGlone, "Changes in neural complexity of the eeg during a visual oddball task," *Clin Neurophysiol*, Vol. 116, pp. 151–159, Jan 2005.

97. van Cappellen van Walsum, A.-M., Y. A. L. Pijnenburg, H. W. Berendse, B. W. van Dijk, D. L. Knol, P. Scheltens, and C. J. Stam, "A neural complexity measure applied to meg data in alzheimer's disease," *Clin Neurophysiol*, Vol. 114, pp. 1034–1040, Jun 2003.

98. Lucia, M. D., M. Bottaccio, M. Montuori, and L. Pietronero, "Topological approach to neural complexity," *Phys Rev E Stat Nonlin Soft Matter Phys*, Vol. 71, p. 016114, Jan 2005.

99. Tononi, G., A. R. McIntosh, D. P. Russell, and G. M. Edelman, "Functional clustering: identifying strongly interactive brain regions in neuroimaging data," *Neuroimage*, Vol. 7, pp. 133–149, Feb 1998.

100. Tononi, G., G. Edelman, and O. Sporns, "Complexity and coherency: integrating information in the brain," *Trends in Cognitive Sciences*, Vol. 2, pp. 474–484, 1998.

101. Jin, S.-H., B.-J. Ham, and S. Y. Kim, "Functional clustering in eeg photic and auditory driving in schizophrenia," *Int J Psychophysiol*, Vol. 56, pp. 249–259, Jun 2005.

102. Burgess, A. P., J. Rehman, and J. D. Williams, "Changes in neural complexity during the perception of 3d images using random dot stereograms," *Int J Psychophysiol*, Vol. 48, pp. 35–42, Apr 2003.

103. Wang, J., H. Rao, G. S. Wetmore, P. M. Furlan, M. Korczykowski, D. F. Dinges, and J. A. Detre, "Perfusion functional mri reveals cerebral blood flow pattern under psychological stress," *Proc Natl Acad Sci U S A*, Vol. 102, pp. 17804–17809, Dec 2005.

104. Tanida, M., K. Sakatani, R. Takano, and K. Tagai, "Relation between asymmetry of prefrontal cortex activities and the autonomic nervous system during a mental arithmetic task: near infrared spectroscopy study," *Neurosci Lett*, Vol. 369, pp. 69–74, Oct 2004.

105. Verberne, A. J., and N. C. Owens, "Cortical modulation of the cardiovascular system," *Prog Neurobiol*, Vol. 54, pp. 149–168, Feb 1998.

106. Cechetto, D., and C. Saper, *Role of the cerebral cortex in autonomic function.* Oxford University Press, 1990.

107. Wittling, W., A. Block, E. Schweiger, and S. Genzel, "Hemisphere asymmetry in sympathetic control of the human myocardium," *Brain Cogn*, Vol. 38, pp. 17–35, Oct 1998.

108. Harmon-Jones, E., "Early career award. clarifying the emotive functions of asymmetrical frontal cortical activity," *Psychophysiology*, Vol. 40, pp. 838–848, Nov 2003.

109. Stark, C. E., and L. R. Squire, "When zero is not zero: the problem of ambiguous baseline conditions in fmri," *Proc Natl Acad Sci U S A*, Vol. 98, pp. 12760–12766, Oct 2001.

110. Gusnard, D. A., M. E. Raichle, and M. E. Raichle, "Searching for a baseline: functional imaging and the resting human brain," *Nat Rev Neurosci*, Vol. 2, pp. 685–694, Oct 2001.

111. Hagemann, D., S. R. Waldstein, and J. F. Thayer, "Central and autonomic nervous system integration in emotion," *Brain Cogn*, Vol. 52, pp. 79–87, Jun 2003.

112. Obrig, H., R. Wenzel, M. Kohl, S. Horst, P. Wobst, J. Steinbrink, F. Thomas, and A. Villringer, "Near-infrared spectroscopy: does it function in functional activation studies of the adult brain?," *Int J Psychophysiol*, Vol. 35, pp. 125–142, Mar 2000.

113. Wobst, P., R. Wenzel, M. Kohl, H. Obrig, and A. Villringer, "Linear aspects of changes in deoxygenated hemoglobin concentration and cytochrome oxidase oxidation during brain activation," *Neuroimage*, Vol. 13, pp. 520–530, Mar 2001.

114. Schroeter, M. L., S. Zysset, and D. Y. von Cramon, "Shortening intertrial intervals in event-related cognitive studies with near-infrared spectroscopy," *Neuroimage*, Vol. 22, pp. 341–346, May 2004.

115. Khoa, T. Q. D., H. M. Thang, and M. Nakagawa, "Testing for nonlinearity in functional near-infrared spectroscopy of brain activities by surrogate data methods," *J Physiol Sci*, Vol. 58, pp. 47–52, Feb 2008.

116. Kershaw, J., K. Kashikura, X. Zhang, S. Abe, and I. Kanno, "Bayesian technique for investigating linearity in event-related bold fmri," *Magn Reson Med*, Vol. 45, pp. 1081–1094, Jun 2001.

117. Huettel, S., "Non-linearities in the blood-oxygenation-level dependent (bold) response measured by functional magnetic resonance imaging (fmri)," *Conf Proc IEEE Eng Med Biol Soc*, Vol. 6, pp. 4413–4416, 2004.

118. Lu, Y., T. Jiang, and Y. Zang, "Single-trial variable model for event-related fmri data analysis," *IEEE Trans Med Imaging*, Vol. 24, pp. 236–245, Feb 2005.

119. Donnet, S., M. Lavielle, and J.-B. Poline, "Are fmri event-related response constant in time? a model selection answer," *Neuroimage*, Vol. 31, pp. 1169–1176, Jul 2006.

120. Aviyente, S., L. A. W. Brakel, R. K. Kushwaha, M. Snodgrass, H. Shevrin, and W. J. Williams, "Characterization of event related potentials using information theoretic distance measures," *IEEE Trans Biomed Eng*, Vol. 51, pp. 737–743, May 2004.

121. Ciftci, K., Y. P. Kahya, A. Akın, and B. Sankur, "Determining hemodynamic response of the brain in the prefrontal region by near-infrared spectroscopy," in *Proc. IEEE 13th Signal Processing and Communications Applications Conference*, pp. 514–517, 2005.

122. Mumford, J. A., and T. Nichols, "Modeling and inference of multisubject fmri data," *IEEE Eng Med Biol Mag*, Vol. 25, no. 2, pp. 42–51, 2006.